HHS Public Access

Author manuscript

Cancer Cell. Author manuscript; available in PMC 2022 March 08.

Published in final edited form as:

Cancer Cell. 2021 March 08; 39(3): 380–393.e8. doi:10.1016/j.ccell.2021.02.003.

A hotspot mutation in transcription factor *IKZF3* drives B cell neoplasia via transcriptional dysregulation

Gregory Lazarian, PhD[1,2,3,*], **Shanye Yin, PhD**[1,4,*], **Elisa ten Hacken, PhD**[1,4,*], **Tomasz Sewastianik, MSc, PhD**[4,5,6], **Mohamed Uduman, PhD**[7], **Alba Font-Tello, PhD**[1,8], **Satyen H. Gohil, MB BS, PhD**[1,9,10], **Shuqiang Li, PhD**[9,11], **Ekaterina Kim, MSc, PhD**[12], **Heather Joyal**[1], **Leah Billington**[1], **Elizabeth Witten**[1], **Mei Zheng**[13], **Teddy Huang**[9], **Mariano Severgnini**[14], **Valerie Lefebvre**[3], **Laura Z. Rassenti, PhD**[15], **Catherine Gutierrez**[1,4], **Katia Georgopoulos, PhD**[16], **Christopher J. Ott, PhD**[17], **Lili Wang, MD, PhD**[18], **Thomas J. Kipps, MD, PhD**[19], **Jan A. Burger, MD, PhD**[12], **Kenneth J. Livak, PhD**[1,9], **Donna S Neuberg, ScD**[20], **Fanny Baran-Marszak, MD, PhD**[2,3], **Florence Cymbalista, MD, PhD**[2,3], **Ruben D. Carrasco, MD, PhD**[4,5,21], **Catherine J. Wu, MD**[1,4,9,#,§]

[1]Department of Medical Oncology, Dana Farber Cancer Institute, Boston, MA [2]INSERM, U978, Université Paris 13, Bobigny, France [3]Laboratoire d'Hématologie, APHP Hôpital Avicenne, Bobigny, France [4]Harvard Medical School, Boston, MA [5]Department of Oncologic Pathology, Dana-Farber Cancer Institute, Boston, MA [6]Dept. of Experimental Hematology, Institute of Hematology and Transfusion Medicine, Warsaw, Poland [7]Center for Immuno-Oncology, Dana Farber Cancer Institute, Boston, MA [8]Center for Functional Cancer Epigenetics, Dana Farber Cancer Institute, Boston, MA [9]Broad Institute of MIT and Harvard, Cambridge, MA [10]Department of Academic Haematology, University College London, London, UK [11]Translational Immunogenomics Lab, Dana-Farber Cancer Institute, Boston, MA [12]Department of Leukemia, The University of Texas MD Anderson Cancer Center, Houston, TX [13]Department of Pathology, Brigham and Women's Hospital, Boston, MA [14]Center for Immuno-Oncology, Dana-Farber Cancer

[#]Correspondence: cwu@partners.org.
[*]These authors contributed equally
[§]Lead contact

AUTHOR CONTRIBUTIONS

G.L, E.T.H, S.Y. and C.J.W. designed and performed the experiments, analyzed data, and wrote the manuscript; T.S, S.L, H.J, L.B., E.W, W.Z., C.G., M.Z, S.P. and V.L., performed experiments; S.Y. analyzed RNA-seq and ChIP-seq data; A.F.T performed ATAC-seq and ChIP-seq experiment. M.U analyzed WGS data. F.C, F.B.M, J.A.B and T.J.K. and L.Z.R. provided CLL patient samples and clinical annotations; S.H.G, S.L, K.J.L. performed bulk RNA-seq and scRNA-seq analysis. M.Z., T.S. and R.C analyzed immunostaining. M.S. performed the Luminex experiments. E.K performed in vitro drug studies. L.W., C.J.O, K.G. and D.N. helped to design and guide the research; D.N. supervised statistical analyses. All authors discussed and interpreted results.

DECLARATION OF INTERESTS

C.J.W. is an equity holder of Biontech, Inc. and receives research funding from Pharmacyclics. C.J.W., D.N. has been a consultant for H3 Biomedicine and received research funding from Celgene. J.A.B. reports receiving grant support and advisory board fees from Pharmacyclics, grant support, advisory board fees, and lecture fees from Gilead, advisory board fees from AstraZeneca, and lecture fees and travel support from Janssen. T.J.K. has received research funding and/or has served as an advisor to Ascerta/AstraZeneca, Celgene, Genentech/Roche, Gilead, Janssen, Loxo Oncology, Octernal Therapeutics, Pharmacyclics/AbbVie, TG Therapeutics, VelosBio, and Verastem. Cirmtuzumab was developed by T.J.K. and licensed by the University of California to Oncternal Therapeutics, Inc., which has provided stock/options to the university and T.J.K. All other authors do not have any relevant conflict of interest.

Institute and Harvard Medical School, Boston, MA, USA [15]Moores Cancer Center, University of California, San Diego [16]Cutaneous Biology Research Center, Massachusetts General Hospital, Charlestown, MA, USA [17]Center for Cancer Research, Massachusetts General Hospital, Harvard Medical School, Boston, MA [18]Department of Systems Biology, Beckman Research Institute, City of Hope National Comprehensive Cancer Center, Monrovia, CA [19]Division of Hematology-Oncology, Department of Medicine, Moores Cancer Center, University of California, San Diego [20]Department of Data Science, Dana-Farber Cancer Institute, Boston, MA [21]Department of Pathology, Brigham and Women's Hospital, Boston, MA

SUMMARY

Hotspot mutation of *IKZF3* (*IKZF3*-L162R) has been identified as a putative driver of chronic lymphocytic leukemia (CLL), but its function remains unknown. Here, we demonstrate its driving role in CLL through a B cell-restricted conditional knock-in mouse model. Mutant *Ikzf3* alters DNA binding specificity and target selection, leading to hyperactivation of B cell receptor (BCR) signaling, overexpression of NF-κB target genes, and development of CLL-like disease in elderly mice with a penetrance of ~40%. Human CLL carrying either *IKZF3* mutation or high *IKZF3* expression was associated with overexpression of BCR/NF-κB pathway members and reduced sensitivity to BCR signaling inhibition by ibrutinib. Our results thus highlight *IKZF3* oncogenic function in CLL via transcriptional dysregulation and demonstrate that this pro-survival function can be achieved by either somatic mutation or overexpression of this CLL driver. This emphasizes the need for combinatorial approaches to overcome *IKZF3*-mediated BCR inhibitor resistance.

Graphical Abstract

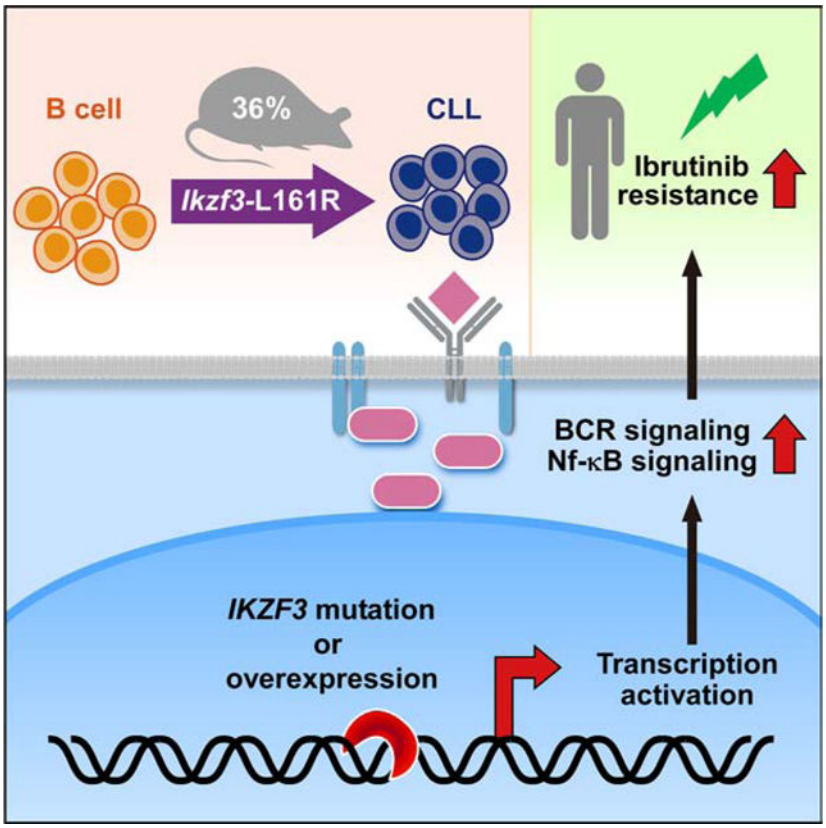

eTOC blurb

Lazarian et al. show that mutation in the transcription factor *Ikzf3* drives CLL development in elderly mice with features reflective of human disease. In human and murine CLL, mutant IKZF3 exerts its oncogenic function by activating BCR and NF-kB signaling, is phenocopied by IKZF3 overexpression, and confers increased B cell fitness upon exposure to BCR signaling inhibitors.

INTRODUCTION

Recent large-scale DNA sequencing studies of chronic lymphocytic leukemia (CLL) have identified a vast array of genetic alterations recurrently mutated in this disease (Landau et al., 2015; Puente et al., 2015), but the functional impact of these lesions remains largely unknown. Included amongst the putative drivers is a hotspot mutation (L162R) in the IKAROS Family Zinc Finger 3 (*IKZF3*, or AIOLOS) gene, which encodes a lymphoid-specific transcription factor essential to B cell development (Morgan et al., 1997). *IKZF3* is mutated in ~3% CLLs and is associated with fludarabine refractoriness (Landau et al., 2015; Morgan et al., 1997). Moreover, the same hotspot mutation has been previously identified in diffuse large B cell lymphoma (DLBCL), mantle cell lymphoma and Waldenström's macroglobulinemia, suggesting its critical role in the malignant transformation of B cells (Bea et al., 2013; Morin et al., 2011; Roos-Weil et al., 2019). In line with this notion, germline knockout of *Ikzf3* in mice has been shown to generate B cell lymphomas (Wang et al., 1998).

IKZF3 contains four zinc-finger domains at its N-terminus that are essential for its binding to a consensus DNA motif a/gGGAA (Georgopoulos et al., 1994; Hu et al., 2016; Molnar and Georgopoulos, 1994); the hotspot mutation is localized within the 2nd zinc-finger domain that makes sequence-specific contacts with DNA. Given the localization of this hotspot mutation at a critical functional domain for transcriptional regulation, we hypothesized that it might interfere with DNA sequence recognition and alter target selection of IKZF3.

Advances in genetic engineering have accelerated the functional interrogation of cancer-associated alterations within *in vivo* models. We used the approach of conditionally knocking in our mutation of interest into the endogenous murine gene locus of *Ikzf3* (Bichi et al., 2002; Klein et al., 2010; Taylor et al., 2019; Yin et al., 2019; Yoshimi et al., 2019). We here demonstrate that expression of *Ikzf3* mutation skews B cell development, enhances B cell activation, and leads to leukemia development in elderly mice. Mechanistically, *IKZF3* mutation directly impacts transcriptional regulation in B cells through altered target DNA recognition, thereby causing deregulated expression of genes involved in key CLL-associated pathways, including B cell receptor (BCR)/NF-κB signaling. Finally, we demonstrate that the insights gleaned from our *in vivo* models are relevant to primary human CLLs. We detect that increased BCR signaling is associated with both mutation or overexpression of *IKZF3*, and that *IKZF3* overexpressing cells have survival advantage upon treatment with the BTK kinase inhibitor ibrutinib. These results demonstrate that IKZF3 overexpression phenocopies the effects of *IKZF3* mutation, and provides selective advantage in the face of BCR inhibition.

RESULTS

Generation of a conditional knock-in mouse model of *Ikzf3* mutation

To investigate the consequences of *IKZF3* mutation *in vivo*, we generated a conditional knock-in mouse model with B cell-restricted expression of the *Ikzf3-L161R* mutation (analogous to human *IKZF3-L162R*) using the *Cd19*-Cre/LoxP system (Figure1A–B, Figure S1A–B). Our breeding strategy yielded cohorts of wild-type (*Cd19*-Cre;*Ikzf3*$^{+/+}$, hereafter *Ikzf3*^{WT}), heterozygous (*Cd19*-Cre;*Ikzf3*$^{fl/+}$, hereafter *Ikzf3*^{Het}) and homozygous mutant (*Cd19*-Cre;*Ikzf3*$^{fl/fl}$, hereafter *Ikzf3*^{Homo}) mice. Presence of the floxed allele was confirmed by targeted PCR of genomic DNA (Figure 1C). We further confirmed that the mutant allele was specifically activated and expressed at ~50% and 100% allelic ratio in cDNA, respectively, in *Ikzf3*^{Het} and *Ikzf3*^{Homo} animals in CD19^{+} expressing cells, as detected by quantitative targeted cDNA pyrosequencing (Figure 1D). Although total protein and nuclear expression were unchanged between the wild-type and mutant *Ikzf3*-expressing lines (Figure 1E, Figure S1C), immunofluorescence staining revealed that mutant IKZF3 forms more speckle-like foci within nuclei than WT-IKZF3 (p=0.02; Figure 1F), indicative of altered physiological properties (Wang et al., 1998).

Ikzf3 mutation alters B cell development and function

We asked whether the *Ikzf3-L161R* mutation alters lymphoid development and function. To this end, we examined B-cell subpopulations within the bone marrow, spleen and peritoneal

cavity in young mice (3 months of age) using multi-parameter flow cytometry (Figure S1D–E). Despite the lack of differences in total splenic B cell counts (Figure S2A), we observed a dramatic decrease in proportions of splenic marginal zone B cells (defined as $B220^{+}$ $CD21^{high}$ $CD23^{-}$) in the *Ikzf3*^{Het} (p=0.005) and *Ikzf3*^{Homo} mice (p=0.002) compared to *Ikzf3*^{WT} mice (Figure 2A, top, Figure 2B). This was further confirmed by immunohistochemical staining of spleen sections (Figure 2A, **bottom**). In parallel, we observed markedly increased proportions of splenic follicular B cells ($B220^{+}$ $CD21^{-}$ $CD23^{high}$) (p=0.02 and p=0.01 in *Ikzf3*^{Het} and *Ikzf3*^{Homo} mice, respectively) (Figure 2A–B). No differences were detected across mouse lines in the splenic T1/T2 subpopulations (Figure S2B), nor in B cell fractions within the bone marrow or peritoneal cavity (Figure S2C–F).

Previous studies have provided evidence for the role of *Ikzf3* in the regulation of germinal center (GC) formation during immune responses (Wang et al., 1998). Upon immunization of 3-month-old mice (n=6 per group) with the T-cell dependent antigen sheep red blood cells (SRBCs), we observed higher proportions of GC B cells in immunized *Ikzf3*^{Homo} compared to *Ikzf3*^{WT} and *Ikzf3*^{Het} mice (p=0.002), suggesting enhanced immune response in the presence of the mutation (Figure 2C–D; Figure S2G). Indeed, higher numbers of $BCL6^{+}$ GCs were detected by immunohistochemical staining of splenic sections from immunized *Ikzf3*^{Homo} mice (Figure S2H). Consistent with the enhanced GC formation in mice with mutated *Ikzf3*, we observed increased plasma cell infiltration in the spleen (Figure 2E, Figure S2I). However, non-immunized mice with mutated *Ikzf3* had decreased levels of serum IgA levels (p≤0.02) suggesting defective immunoglobulin class switching in presence of the mutation (Chaudhuri and Alt, 2004), and a trend towards increased serum level expression of IL-5 (Figure S2J–K), previously implicated in IgA production (Schoenbeck et al., 1989).

Since activation of B cell receptor (BCR) signaling is known to lead to enhanced generation of follicular rather than MZ B cells (Cariappa et al., 2001), we asked whether *Ikzf3*-L161R could alter BCR signal transduction. Indeed, immune stimulation of splenic B cells (with anti-IgM antibodies for 5 and 15 minutes) induced strong upregulation of phosphorylated SYK, AKT and ERK kinases in B cells from both *Ikzf3*^{Het} and *Ikzf3*^{Homo} mice compared to those from wild-type mice, with a more dramatic activation in *Ikzf3*^{Homo} than in *Ikzf3*^{Het} mice (Figure 2F; Figure S2L). Moreover, higher calcium flux following BCR crosslinking was detected in *Ikzf3*^{Het} and *Ikzf3*^{Homo} B cells compared to wildtype controls (p=0.05 and p=0.04, respectively, Figure 2G–H), consistent with enhanced responsiveness to anti-IgM.

Ikzf3 mutation induces CLL-like disease in elderly mice

To determine whether *Ikzf3* mutation directly drives CLL generation, we monitored the peripheral blood of three cohorts of mice (*Ikzf3*^{WT}, *Ikzf3*^{Het} and *Ikzf3*^{Homo}, n=30 each) by flow cytometry on a bi-monthly basis for the accumulation of $B220^{+}CD5^{+}$ CLL-like cells, starting from 6 months of age. No circulating CLL-like cells were observed in any *Ikzf3*^{WT} mice up to 24 months of age (Figure 3A). However, for 11 of 30 (36%) *Ikzf3*^{Het} mice and for 3 of 30 (10%) *Ikzf3*^{Homo} mice, we detected clonal $B220^{+}CD5^{+}Ig\kappa^{+}$ CLL-like cells comprising up to 10–50% of total circulating cells between 18 and 24 months of age (Figure

3A–B; Figure S3A), confirming the role of mut-*IKZF3* as a CLL driver. Mut-*Ikzf3* CLL-like splenocytes also expressed CD23, to a greater extent than Eμ-TCL1- derived splenocytes (p=0.02, Figure S3B) (Efanov et al., 2010). CD23 is downregulated in more aggressive CLL cases (Woroniecka et al., 2015), and hence our findings are consistent with the indolent nature of our mouse model.

Mice with CLL-like disease consistently displayed enlarged spleens (Figure 3C) with high infiltration of the spleen (30–80%) and peritoneal cavity, but only minimal marrow involvement. This suggested a preferential homing of the *Ikzf3* mutant B cells to the splenic microenvironment, which we confirmed by CD5/PAX5 IHC immunostaining of tissue sections (Figure 3D–E). Two of 30 (6%) *Ikzf3*^{Het} mice displayed an enlarged spleen without evidence of circulating disease. By H&E staining of spleen sections from these mice, the cellular morphology of the infiltrated tumor cells was consistent with diffuse large B cell lymphoma (DLBCL). Moreover, immunostaining of these sections revealed the expression of BCL6 and a high Ki-67 index, consistent with DLBCL rather than CLL (Figure S3C–F). IGHV sequence analysis of isolated B cell fractions from blood or spleen revealed that all CLL-like cells clonally expressed unmutated IGHV genes (100% homology with germline), similar to human mut-*IKZF3* CLL, whereas the DLBCL cases carried somatically mutated IGHV. Remarkably, we noticed that CDR3 sequences of 2 of the CLL mice showed identical CDR3 length and 60–90% amino acid similarity with those of BCRs from the Em-TCL1 (Yan et al., 2006) and the MDR CLL mouse models (Klein et al., 2010) (Table S1). In the 2 DLBCL cases, the absence of prior detection of circulating clonal CD5^{+} B cells and the expression of IGHV somatically mutated genes, which typically occurs in *de novo* DLBCL, excluded Richter's transformation. We further confirmed the ability of splenocytes derived from 5 CLL-*Ikzf3*^{Het} mice to engraft into both congenic immunocompetent (CD45.1) and immunodeficient (NSG) secondary hosts. CLL-like cells were detectable in the peripheral blood of NSG and CD45.1 recipient mice, respectively 4 and 20 weeks following transplant (Figure S3G–J), with NSG transplants experiencing shorter overall survival than CD45.1 recipients (p=0.0035, Figure S3K).

Ikzf3 mutation alters DNA binding and target selection in pre-leukemic mice

To determine transcriptional dysregulations already occurring at the pre-leukemic stage that could favor the generation of CLL, we performed RNA-seq analyses on purified splenic B cells from *Ikzf3*^{Homo} compared to the *Ikzf3*^{WT} mice (3-months old, n=3 per cohort). Altogether, we identified a total of 402 significantly upregulated and 742 significantly downregulated genes in the *Ikzf3*^{Homo} compared to *Ikzf3*^{WT} mice (Figure 4A, Fold-change>2, False Discovery Rate FDR<0.05; Table S2). Gene Ontology (GO) of these differentially expressed signatures revealed enrichment in processes involved in immune regulation (i.e. innate and adaptive immune system, cytokine production, calcium homeostasis) and cell migration (i.e. leukocyte migration, MAPK signaling, angiogenesis) (Figure 4B, Table S2). In addition, gene set enrichment analysis (GSEA) revealed *Ikzf3*^{Homo} B cells to have an expression signature typical of B cells residing within the light zone of germinal centers and downregulation of signatures related to BCR signaling inhibition by BTK knockout (Cancro et al., 2001), consistent with hyperactivation of BCR signaling in those cells (Figure 4C).

Given the localization of the hotspot mutation within the DNA binding domain, we asked whether this mutation can alter the DNA binding specificity of IKZF3 protein. To this end, we performed chromatin immunoprecipitation followed by deep sequencing (ChIP-seq) of IKZF3 in *Ikzf3*^{Homo} versus *Ikzf3*^{WT} splenic B cells (n=5 mice pooled per genotype). As shown in Figure 4D, we detected a strong recruitment of both WT and mut-IKZF3 to transcription start sites (TSS), consistent with the critical role of IKZF3 in transcriptional regulation. In total, we identified 3794 and 2795 highly confident IKZF3 peaks from *Ikzf3*^{WT} and *Ikzf3*^{Homo} cells, respectively (>2-fold enrichment and FDR<0.001, Table S3). Only 910 of 2795 (33%) peaks associated with *Ikzf3*^{Homo} cells were shared with the *Ikzf3*^{WT} cells (Figure 4E-**left**), indicating altered DNA binding specificity in the presence of the mutation. Two dominant DNA binding motifs were found across the high confidence peaks identified for the *Ikzf3*^{WT} cells, including the canonical IKAROS family motif [AGGAAGTG], as well as an [ACAGGA] motif, which accounted for a large fraction of the peaks (54% and 38% of all peaks, respectively). Notably, although the IKZF3 peaks in the *Ikzf3*^{Homo} cells were mostly enriched for the same two dominant motifs, the DNA sequences of these motifs became degenerate (Figure 4E-**right**), suggesting that *Ikzf3-L161R* can alter IKZF3 DNA sequence recognition and target selection.

KEGG pathway analysis revealed that the ChIP-seq targets of both *Ikzf3*^{WT} and *Ikzf3*^{Homo} cells were most significantly enriched for BCR signaling genes (covering 50–60% of direct targets) (Figure 4F; Table S3). Mut-IKZF3 targets were also enriched for several migration-related pathways (e.g. focal adhesion, leukocyte migration), which might explain the specific homing property of the CLL-like cells. To identify targets directly affected by mut-IKZF3, we integrated the ChIP-seq and RNA-seq data using Cistrome-GO (Li et al., 2019), which ranks target genes by considering both mut-IKZF3 binding strength and the change in gene expression. Strikingly, our results revealed that genes with the highest likelihood to be true direct targets of mut-IKZF3 (i.e. high Cistrome-GO rank) were mostly upregulated (Figure 4G–H), including 22 of the top 25 direct targets (Figure 4I; Table S3 for full list), supporting the role of mut-IKZF3 as a transcriptional activator. To investigate the potential of mut-IKZF3 binding to alter local histone modifications or chromatin structure, we performed ChIP-seq of several histone marks (i.e., H3K4me2, H3K4me3 and H3K27ac) and ATAC-seq. IGV tracks of the ChIP-seq, ATAC-seq and RNA-seq signals for the top three Cistrome-GO targets are shown in Figure 4J. These included *Nfkbid*, a putative regulator of NF-kappa-B signaling (Meijers et al., 2020; Touma et al., 2011), also known to be upregulated in the CLL Eμ-TCL1 mouse model (Zanesi et al., 2013)*; Tagap*, a Rho GTPase-activating protein (Tamehiro et al., 2017); and *Jun*, an oncogenic transcription factor and a member of the BCR signaling pathway.(Foletta et al., 1998) In all three cases, mut-IKZF3 bound to the nucleosome-free regions, which were otherwise poorly recognized by WT-IKZF3, in the TSS of the target genes and activated their expression. Conversely, reduced mutant-IKZF3 binding to TSS was in some instances associated with downregulation of target genes (Figure S4A). In contrast, the impact of mut-IKZF3 on histone modifications or chromatin structure around gene promoters was minor, both at the global level (Figure S4B) or when limited to the analysis of the top 100 Cistrome-GO targets (Figure S4C). These results indicate that the gene expression dysregulation associated with mut-IKZF3 is the result of the direct gene transactivation mediated by mut-IKZF3 binding at gene target promoter

regions rather than a broader epigenetic dysregulation. We confirmed the overexpression of *Nfkbid, Tagap* and other highly ranked targets in the mut-IKZF3 expressing mouse lines by quantitative real-time PCR (Figure S4D).

Included among the top targets was the chemokine receptor *Cxcr4*, which was recently shown to be regulated by *IKZF3* in lung cancer (Li et al., 2014). Given the known critical role of the CXCR4/SDF1α axis in CLL for leukemic cell homing and interaction with the microenvironment (Burger et al., 1999), we tested the effects of mut-*Ikzf3* on the *in vitro* chemotaxis of mouse B cell splenocytes using a transwell-based chemotaxis assay. From these studies, we observed increased migration of $Ikzf3^{Homo}$ cells toward SDF1α (the cognate ligand for CXCR4 receptor) compared to $Ikzf3^{wt}$ and $Ikzf3^{Het}$ ($p<0.001$, Figure S4E). Together, these data suggest that *Ikzf3-L161R* functions as a gain-of-function mutation that alters target selection and activates transcription, with an impact on core B cell functions including activation of BCR signaling and enhancement of cellular migration.

Ikzf3-L161R activates BCR and NF-κB signaling in CLL-like cells

To determine the molecular events contributing to CLL development, we performed transcriptome analysis of FACS-purified CLL-like cells ('CLL', n=5 [4 $Ikzf3^{Het}$, 1 $Ikzf3^{Homo}$], collected at a median of 15 months of age) and non-CLL B cells from the same mice ('non-CLL', n=4 [3 $Ikzf3^{Het}$, 1 $Ikzf3^{Homo}$]), as well as normal B cells from age-matched WT animals ('WT', n=3) (Figure 5A). Of note, we confirmed the presence of the *Ikzf3* hotspot mutation in all CLL samples (Figure S5A). PCA analysis revealed strikingly distinct gene expression profiles amongst CLL-like cells, while non-CLL B cells with or without the mutation were relatively more similar (Figure 5B, Figure S5B). When focusing on the most commonly deregulated events in the CLL-like cells, we identified 598 significantly upregulated genes and 267 downregulated genes compared to WT B cells (FC>2, FDR<0.05); these were assigned into 4 distinct clusters based on their expression levels in mut- and wild-type B cells (Figure 5C, Table S4). Cluster I genes were significantly upregulated in the CLL-like cells compared to both WT and non CLL-B cells, while Cluster II genes were upregulated in the non-CLL B cells collected from the mut-*Ikzf3* animals compared to WT B cells and the CLL-like cells. Cluster III genes were consistently downregulated in CLL-like cells and non CLLB cells compared to WT B cells; Cluster IV genes were only downregulated in CLL-like cells. Of note, 29 of 30 (96%) genes significantly activated by *Ikzf3-L161R* in the pre-leukemic animals (3-month-old) were also significantly upregulated in CLL-like cells (Figure 5C, black lines on right), including *Nfkbid* and *Myc*. Cluster I genes were highly enriched for key regulators of B cell regulation (i.e. lymphocyte activation, proliferation, and calcium-mediated signaling), as we observed in the young pre-leukemic mice (Table S4). Downregulated genes in CLL (Cluster III/IV) were enriched for lymphocyte differentiation, adaptive immune response and autophagy, which may be also highly relevant to CLL generation.

We noted a general upregulation of BCR signaling genes in CLL-like cells (Figure 5D) compared to the non-CLL B cells from the same animals, including *Lyn* kinase, and the cytoskeletal modulators *Vav2* and *Rac2* (Figure 5E), supporting hyper-activation of BCR signaling as a pathogenic mechanism favoring leukemogenesis (Table S4). Moreover,

prediction of transcription factors (TFs) associated with Cluster I genes using Enrichr (Kuleshov et al., 2016) revealed a unique role for *NFKB1*, which putatively activates transcription of 23% of Cluster I genes (Figure 5F, p=0.002), supporting hyperactivation of the BCR/NF-κB signaling axis and the downstream transcriptional network in CLL-like cells. We confirmed upregulation of VAV2 and RAC2 at the protein level, and also LYN kinase (Figure S5C, $p<0.05$). In line with this notion, we also observed enhanced phosphorylation of BCR-associated kinases (LYN, SYK, ERK, AKT) and NF-κB signaling (P65) in response to anti-IgM in CLL-like cells by western blot (Figure 5G, Figure S5D).

Notably, our ChIP-seq data generated from pre-leukemic mice provided evidence of a new binding site for mut-IKZF3 at the LYN promoter, potentially explaining the increased expression of LYN in *Ikzf3*-mutant cells (Figure 5H). In support of the idea that LYN activity might be essential for cell survival through activation of BCR signaling, we observed increased cell death of mut-*Ikzf3* CLL cells following exposure to the dual LYN/BCR-ABL inhibitor bafetinib (p=0.02) compared to ibrutinib or rapamycin (p=0.001) (BTK kinase and mTOR inhibitors, respectively). We also observed a trend towards decreased viability following exposure to the gamma-secretase inhibitor PF308414, which targets NOTCH signaling (Figure 5I). Of note, increased sensitivity to bafetinib was exclusive to the *Ikzf3* mouse model, as cells from other CLL mouse models (i.e., Eμ-TCL1, MDR) showed lower sensitivity to the drug (Figure S5E). We thus suggest a model in which mut-*Ikzf3* transcriptionally upregulates the early kinase LYN that in turn supports the hyperactivation of the oncogenic BCR/NF-κB signaling axis to drive CLL generation and sustain leukemic cell survival.

The long latency of our mouse model led us to query whether CLL-like cells carried additional genetic alterations. We therefore performed whole-genome sequencing of DNA isolated from 5 CLL mice (4 $Ikzf3^{Het}$, 1 $Ikzf3^{Hom}$) and 2 DLBCLs, as well as matched germline DNA (Table S5). Across all 5 mice with CLL, we observed consistent amplification of chromosome (Chr) 15 (Fig. 5J). In line with this copy number change, most of the genes on Chr15 were upregulated in CLL cells compared to normal B cells (Figure 5K), including the *Myc* oncogene (Figure 5L, Figure S5F). Additional alterations included Chr17, amplified in 3 of 5 CLL mice, and a partial amplification of Chr2 in a region that encompasses *Notch1*, a recurrent CLL driver (Landau et al., 2015). Copy number variations were more diverse in the 2 mice with DLBCL (Figure S5G), confirming the distinct evolutionary trajectories of the CLL *vs.* DLBCL disease entities.

IKZF3 mutation upregulates BCR signaling genes in human CLL

To determine the influence of mut-*IKZF3* on global gene expression in human CLLs, we evaluated 10 CLL samples by RNA-seq (mut-*IKZF3* [n=4], WT-*IKZF3* [n=6]). All patients were IGHV unmutated and carrying clonal *IKZF3* mutations (*IKZF3* mutant allele frequency >40%) (Table S6). Altogether, we observed 279 significantly upregulated and 317 downregulated genes in CLLs with mut-*IKZF3* versus WT (Figure 6A, FC>2 and FDR<0.05, Table S6). We identified 6 consistently upregulated genes and 3 consistently downregulated genes between mouse and human CLLs carrying the *IKZF3* mutation using stringent cut-offs (FC>2, FDR<0.05). Using a less stringent cutoff for differential gene

expression ($p<0.05$), we could find 204 consistently upregulated genes and 31 consistently downregulated genes, in line with the role of mut-*IKZF3* as a transcriptional activator (Table S6). Notably, consistent with the murine data, we found mut-*IKZF3* to be associated with an increased BCR signaling gene expression signature in human CLLs (Figure 6B), and upregulation of key regulators, including the co-receptor *CD79A*, and the *AKT2* and *PIK3CA* kinases (Figure 6C).

We previously reported that CLLs with *IKZF3* mutation appeared to increase in cancer cell fraction (CCF) with resistance to fludarabine-based chemotherapy (Landau et al., 2015). Others have shown an instance of increase in mut-*IKZF3* CCF upon treatment with the BCR signaling inhibitor ibrutinib (Ahn et al., 2019). These studies together suggest an association of *IKZF3* mutation (and increased BCR signaling) with increased cellular survival following either chemotherapy or targeted treatment. Since somatic mutation represents but one mechanism by which a driver cellular pathway can be altered (Wang et al., 2016; Yin et al., 2019), we examined whether aberrant expression of IKZF3 could also yield differences in BCR signaling. We noted that prior investigations revealed the expression of *IKZF3* to be variable across CLL samples (Billot et al., 2011; Duhamel et al., 2008; Nuckel et al., 2009); we thus examined *IKZF3* expression and BCR signaling gene expression, or the 'BCR score' (calculated as the mean expression of 75 BCR signaling-associate genes) (Yin et al., 2019) in two independent human CLL cohorts characterized by RNA-seq (DFCI cohort, n=107; ICGC cohort, n=274) (Ferreira et al., 2014; Landau et al., 2014). *IKZF3* expression was positively correlated with BCR score (Figure S6A), and CLLs with high *IKZF3* expression had higher BCR scores than those with low *IKZF3* expression ($p\leq0.0015$; Figure 6D). These findings were consistent with the idea that *IKZF3* may act as a broad regulator of BCR signaling genes, and that *IKZF3* overexpression, like *IKZF3* mutation, can putatively provide selective advantage to CLL. In support of this notion, our re-analysis of a gene expression dataset of 107 newly diagnosed CLL samples (Herold et al., 2011) revealed that high *IKZF3* expression is associated with worse overall survival ($p=0.035$; Figure 6E).

To determine whether high expression of *IKZF3* is associated with altered sensitivity to ibrutinib, we performed scRNA-seq analysis of 2 previously treatment-naïve patients undergoing ibrutinib therapy (paired samples, baseline *vs.* Day 200) (Fig. 6F, Table S6). As shown in Figure S6B, amongst the various categories of mononuclear cells identified within the peripheral blood, *IKZF3* was mainly expressed in CLL cells and T cells. Consistently, after ibrutinib treatment, residual CLL cells in both patients showed elevated *IKZF3* expression compared to Day 0 (both $p<0.0001$, Figure 6G), whereas no such change was observed in T cells, indicating selection of CLLs with high *IKZF3* expression upon ibrutinib exposure. Expression levels of several key regulators of BCR signaling (including *CD79B, LYN, FOS, RAC1* and the NF-κB regulators *PRKCB* and *NFKBIA*) were likewise upregulated (Figure 6H), in line with the notion that *IKZF3* is a master regulator of BCR signaling gene expression. Some of these genes, including LYN and FOS, also appeared to be amongst the most upregulated in presence of mut-IKZF3 (Figure 6C). Altogether, these data implicate that increased BCR signaling, associated with either *IKZF3* mutation or overexpression, may facilitate increased cellular fitness in the face of exposure to BCR signaling inhibitors.

Given the enhanced BCR signaling in patients with high *IKZF3* expression or with mutated *IKZF3*, we asked whether these featured were linked to differential sensitivity of primary CLL cells to BCR inhibition by ibrutinib. In fact, we observed poorer viability after *in vitro* exposure to ibrutinib in CLL cells with either high *IKZF3* expression or mutated *IKZF3* compared to cells expressing IKZF3 at lower levels (p=0.005), irrespective of IGHV mutation status (Figure 6I).

DISCUSSION

Herein, we report the generation of a CLL mouse line modeled upon a hotspot mutation found in human CLL that recapitulates the cardinal features of this leukemia. Mut-*Ikzf3* CLL mice display pathologic features consistent with human disease, exhibit relatively indolent growth (~15–18 months onset), and express the heterozygous mutation; altogether, these data provide functional evidence that mut-*IKZF3* is a CLL driver. Whereas *IKZF3* is mostly known to act as a transcriptional repressor through recruitment of HDACs to target genes via its C-term protein interaction domains (Koipally et al., 1999), we here uncover a mechanism linking altered gain-of-function by *IKZF3* via mutation within its N-term DNA binding region. In particular, we demonstrate that this mutation results in altered DNA binding to BCR signaling-related target genes, leading to their transactivation, and to enhanced BCR responsiveness. Our findings thus complement older studies demonstrating that *IKZF3* germline knock-out mice exhibit increased BCR-mediated proliferative responses (Wang et al., 1998), again highlighting the likely negative regulatory function of *IKZF3* in normal B cell development. One paradox observed in this study is the more pronounced phenotype observed in heterozygous mutant rather than homozygous mutant mice. In human disease, *IKZF3* mutation is solely observed as heterozygous events. We speculate that homozygous *Ikzf3* mutation may cause decreased B cell fitness. A potential explanation includes a dose effect of mut-*Ikzf3*-associated hyperactivation of the BCR signaling above maximum thresholds of signaling strength, which may facilitate negative B cell selection, rather than lymphomagenesis, as previously postulated (Muschen, 2018).

Our findings underscore a key role of *IKZF3* in BCR-associated oncogenesis. BCR signaling has been extensively described as a cardinal pathway contributing to CLL leukemogenesis, both in *in vitro* primary CLL-based model systems (Burger et al., 2000), and *in vivo*, in the Eμ-TCL1 mouse model (Iacovelli et al., 2015). One of the strongest prognostic markers of CLL, unmutated immunoglobulin gene usage, is associated with greater BCR signaling proficiency (Lanham et al., 2003) and links increased BCR signaling responsiveness with a more dismal clinical outcome of patients (Damle et al., 1999; Hamblin et al., 1999). In our *in vivo* model, we observed enrichment in BCR signaling gene expression at the pre-leukemic stage, suggesting that dysregulation in the BCR signaling circuitry may be an early event favoring transformation of mut-*Ikzf3* normal B cells into CLL. We found evidence of LYN kinase, one of the earliest kinases within the BCR signaling pathway (Yamanashi et al., 1991), as a target of mut-*Ikzf3* and the essentiality of LYN kinase activity for survival of mut-*Ikzf3* CLL cells. All of our mut-*Ikzf3* CLL-mice carried unmutated immunoglobulins and enhanced responsiveness to BCR stimulation compared to non-CLL mut-*Ikzf3* B cells, again highlighting BCR signaling competence as a key feature underlying transformation and progression. Remarkably, we found CDR3

regions of mutant-*Ikzf3* BCRs to be near-identical to those of BCRs from Eμ-TCL1 mice also previously described to show high BCR competence (Yan et al., 2006), and from MDR mice (Klein et al., 2010), suggesting similar mechanisms of BCR ontogeny and clonal selection in these independent mouse models. Amongst the most significantly altered genes, we identified members of the BCR signaling and migration pathways. Of note, WGS analysis revealed the presence of additional oncogenic hits in *Ikzf3*-mutant CLLs, namely amplification of chromosome 15, which was also detected in our previously reported double mutant *Sf3b1/Atm* CLL mice (Yin et al., 2019) and associated with upregulation of MYC, suggesting commonalities of mechanisms driving disease evolution in independent models.

Insights from prior studies have suggested that core cancer pathways can be impacted via different mechanisms of deregulation (Wang et al., 2016). We already noted that *IKZF3* mutation is selected in fludarabine-based regimens (Landau et al., 2015) and was reported to be selected in one patient experiencing ibrutinib resistance (Ahn et al., 2019). Although *IKZF3* mutation has been identified in patients' samples at a relatively low frequency (~3%), (Landau et al., 2015) we have observed expression of the *IKZF3* gene to be variably dysregulated amongst CLL patients. Through re-analysis of transcriptomic data from 2 cohorts of human CLL (DFCI and ICGC) (Ferreira et al., 2014; Landau et al., 2014), we have here shown a strong positive correlation between *IKZF3* and BCR signaling gene expression, suggesting that deregulated *IKZF3* expression phenocopies *IKZF3* mutation in relation to BCR signaling regulation in human CLL. In support of this notion, we identified the association between increased *IKZF3* expression and reduced overall survival of previously untreated CLL patients (in the pre-novel agent era), and furthermore, evidence of increased cellular fitness following ibrutinib exposure. In the context of ibrutinib treatment, we not only observed increased expression of *IKZF3* and of genes found to be upregulated in *IKZF3*-mutant samples (i.e. *FOS* and *RAC1*), but also reduced sensitivity to BCR inhibition by ibrutinib in either *IKZF3* high expressors or *IKZF3*-mut samples. These results again suggest that *IKZF3* expression can to some extent phenocopy *IKZF3* mutation.

IKZF3 overexpression has similarly been proven essential for multiple myeloma cell growth (Lu et al., 2014), and has been implicated in mantle cell lymphoma resistance to ibrutinib (Dobrovolsky et al., 2019). Altogether, these studies support the oncogenic functions of *IKZF3* in CLL and across a range of B cell malignancies. As a strategy to overcome IKZF3-driven drug resistance, efforts have been made to develop novel small molecule inhibitors simultaneously targeting IKZF3 and BTK, with promising activity in MCL (Dobrovolsky et al., 2019). The BH3 mimetic venetoclax could also be an alternative strategy to overcome *IKZF3* driven drug resistance. Identification of mutation or overexpression of *IKZF3* could therefore identify patients who can benefit of combination or venetoclax-based therapy.

STAR METHODS

RESOURCE AVAILABILITY

Lead Contact—Further information and requests for resources and reagents should be directed to and will be fulfilled by the Lead Contact, Catherine J. Wu (cwu@partners.org).

Materials Availability—The mouse strain will be available at the Jackson Laboratory Repository with the JAX Stock no. 035514 (http://jaxmice.jax.org/query)

Data Software Availability—The raw and processed RNA-seq and ATAC-seq data described in this publication have been deposited in NCBI's Gene Expression Omnibus (GEO) -- Accession number: GSE143711. Human RNA-seq and gene expression data have been submitted to NCBI's Database of Genotypes and Phenotypes (dbGaP; https://www.ncbi.nlm.nih.gov/gap) under study number phs2335.v1.

EXPERIMENTAL MODEL AND SUBJECT DETAILS

Primary Human Samples—All primary CLL samples were obtained from Avicenne Hospital (Assistance Publique-Hôpitaux de Paris, Bobigny, France), from the University of Texas M.D. Anderson Cancer Center (MDACC) or from the CLL Research Consortium (CRC). All specimens were collected following informed consent from patients in accordance with the principles of the Declaration of Helsinki and with the approval of the Institutional Review Boards (IRB) of Avicenne Hospital, MDACC and CRC. Clinical characteristics of patients from whom samples were collected are reported in Table S6. CLL cells were isolated from peripheral blood using the Ficoll method, and flow cytometry analysis confirmed leukemia purity of >80% in all cases. Cells were either used fresh or cryopreserved in 10% DMSO until the time of analysis.

Mouse model—All animal protocols were approved by the Institutional Care and Use Committee of the Dana-Farber Cancer Institute (DFCI). Based on the homology between the human and murine IKZF3 amino acid sequences and given the high conservation of the DNA binding domain across the two species, *Ikzf3* L161R floxed mice (*Ikzf3*$^{fl/+}$) on C57BL/6 background were generated to model the human L162R mutated site (Biocytogen, MA). The floxed allele was designed so that the cDNA sequence of the exons 5 to 8 and a stop codon were flanked by two LoxP sequences and inserted after the fourth exon of the endogenous *Ikzf3* locus. Exon 5 containing the L161R mutation followed by the exons 6 to 8 were placed downstream of the 2nd LoxP sequence. In the presence of the Cre recombinase, the sequence between the LoxP sequences is removed, allowing the expression of the *Ikzf3* mutant allele. To obtain B-cell-specific *Ikzf3*- L161R mutation expression, *Cd19*-Cre/Cre mice were crossed with the *Ikzf3*$^{fl/+}$ mice. The offspring from this breeding gave wild-type mice *Cd19-Cre;Ikzf3*$^{+/+}$ (*Ikzf3*^{WT}) and heterozygous mutant mice *Cd19-Cre;Ikzf3*$^{fl/+}$ (*Ikzf3*^{Het}) simultaneously. We then bred the heterozygous mutant mice with *Ikzf3*$^{fl/fl}$ mice to obtain homozygous mutant mice *Cd19-Cre;Ikzf3*$^{fl/fl}$ (*Ikzf3*^{Homo}).

METHOD DETAILS

Mouse genotyping—Genotypes were confirmed by PCR of genomic DNA from tail using a set of primers targeting the floxed allele (Forward A1-LoxP: 5'-CTTGACTCTGTGAGTCCGTTTTGC and Reverse A2-LoxP: 5'-CAGTGACACAGATCGCTTGGGAAC). This reaction amplifies a wild-type product of 217 bp and a second PCR product of 281 bp corresponding to the floxed allele. Activation of the floxed allele by the Cre recombinase was confirmed by PCR on genomic DNA from purified B cells and non-B cell fractions using a set of primers that amplifies the activated allele

(Forward B2: 5'TGCTGCTCTCCAGACACAAGGC and Reverse mFl1: 5'TCATGATGAGTCCCATGCCACGC Reverse). This reaction amplifies a wild-type product of 880 bp and a second PCR product of 907 bp corresponding to the activated allele. The PCR products were run on a 2% gel with a 100 bp ladder as reference. Presence of the activated allele was detected only in the purified B cell fraction.

Pyrosequencing—Relative transcript expression of the mutant allele compared to the wild-type was quantified by cDNA pyrosequencing, as previously described(Yin et al., 2019). Biotinylated amplicons generated by PCR of transcripts surrounding *Ikzf3* L161R mutation were generated. Immobilized biotinylated single stranded DNA fragments were isolated per the manufacturer's protocol (PyroMark Gold Q96, Qiagen, Valencia, CA) and sequencing undertaken using an automated pyrosequencing instrument (PSQ96; Qiagen, Valencia, CA), followed by quantitative analysis using Pyrosequencing software (Qiagen). Forward (5'ATCAGTGTGGGGCATCTTT) and reverse (5'Bio-TTTTCCCCTGTGTGCAGTTTAA) primers were used to amplify the region across the L161R mutation site from the cDNA; the probe sequence was 5'TACTCAGAAAGGTAACCTC.

Disease blood monitoring in mouse cohorts—Mice were monitored monthly from the age of 3 to 24 months of age. 100 μl of blood was collected from mice into EDTA-containing tubes via submandibular bleed. Erythrocyte lysis was carried out by incubating the blood in 1 ml of ACK buffer for 5 min and then washing with PBS supplemented with 2% FCS and 2 mM EDTA. The cells were then stained with a cocktail of antibodies against CD5-FITC, B220-Pacific Blue, CD11b-APC-Cy7, CD3-APC and Igκ-PE for 15 min at 4°C. Cells were then washed and analyzed using flow cytometry.

B cell purification—Mice were euthanized in a CO_2 chamber and harvested spleens or femurs were mechanically dissociated to form a single cell suspension. Erythrocyte lysis was carried out using ACK buffer and B cells were immunomagnetically selected from the resulting cell suspension using the MACS mouse B cell Isolation Kit (Miltenyi Biotec, Bergish Gladbach, Germany). B cell purity was confirmed post-sorting on a FACS Canto I instrument using the flow cytometry staining procedures described above, and were at least 85% pure, but typically >90%.

Immunohistochemistry and Immunofluorescence—All spleens were fixed in 10% buffered neutral formalin overnight (Fisher Scientific, Waltham, MA), followed by 70% ethanol until the tissues were processed. Spleens were then paraffin-embedded and sectioned into 20μm for IHC staining. Hematoxylin and Eosin staining, BCL6, BCL2, KI-67, CD19, IgM, B220, and CD5 immunostaining were performed on the section using standard procedures. Purified B cells from mouse spleens were cytospun on glass slides at a density of 1×10^6 cells/ml in 200μl PBS+ 10% FCS, fixed in 4% paraformaldehyde at room temperature for 15min, wash 3 times in PBS+ 0.1% Tween-20, permeabilized 5 min in PBS + 0.1% TritonX-100 and blocked 1h in PBS+0.1% Tween-20 supplemented with 5% FCS. Cells were incubated overnight at 4°C with the primary murine antibody anti-IKZF3 (clone: 8B2, Ebioscience). The following day, the slides were washed 3 times in PBS+ 0.1%

Tween-20, incubated with the secondary antibody anti-mouse conjugated to Alexa488 for 1h at room temperature, washed 3 times and the nuclei were counterstained with DAPI. Coverslips were mounted onto glass slides in Vectashield (Vectorlabs, Clinisciences, Montrouge, France) and visualized on a confocal microscope Leica. ImageJ software was used for foci quantification per nuclei. 100 nuclei were analyzed per condition from 10 different fields.

B cell subpopulation analysis—The proportion of the cell subpopulations from the bone marrow, the spleen and the peritoneal cavity was analyzed by flow cytometry based on the expression of surface markers. Cells from the bone marrow or the spleen were extracted by mechanic dissociation, and erythrocytes lysis was carried out with ACK lysis buffer. Cells were washed in with PBS supplemented with 2% FCS and 2mM EDTA and incubated with antibodies cocktail for 15minutes at 4°C. Cell suspensions prepared from spleen were stained with the following antibodies (all purchased from BioLegend, San Diego, CA): antibodies anti-B220-BV421, CD93-BV650, anti-CD23-BV786, anti-CD21-BV510, anti-IgD-APC.Cy7 and anti-IgM-PE.Cy7 for marginal zone B cells, follicular B cells and transitional B cells quantification; marrow cell suspensions were stained with anti-CD43-PE, anti-IL-7R-BV711, anti-CD93-BV650, anti-B220-BV421, anti-CD11b-PerCP.C5.5, anti-TER-119-PerCP.C5.5, anti-CD3e PerCP.C5.5, anti-Ly6G/Ly6C PerCP.C5.5, anti-IgD-APC.Cy7 and anti-IgM-PE.Cy7 for pro-B cells, pre-B cells, immature, transitional and mature B cells quantification; and peritoneal cavity cells with anti-CD5-FITC, anti-B220-PacificBlue and anti-CD11b-APC.Cy7 antibodies for B1a cells quantification.

For germinal centers generation analysis, mice of 8–12 weeks were immunized intraperitoneally with 10^9 sheep red blood cells (Immunoresearch) in 150 microliters PBS. Spleens were collected 10 days after immunization and analyzed by flow cytometry to quantify germinal center B-cells using a combination of anti-B220-BV421, anti-CD95-PE and anti-CD38-APC antibodies and plasma cells with anti-CD138-BV421, anti-TACI-PE, anti-B220-PerCP.Cy5.5 and anti-CD19-APC.Cy. Spleen sections were analyzed by immunohistochemistry and stained with anti-BCL6 antibody for germinal centers and with anti-CD138 for plasma cells detection.

BCR stimulation and Western Blot analysis—For analysis of BCR signaling transduction, purified splenic B-cells (3×10^6) were stimulated in 1ml RPMI 1640 medium (Life Technologies, Woburn, MA) supplemented with 10% FCS, and 1% penicillin/streptomycin in the presence of 10μg/ml goat anti-mouse IgM (Southern Biotech, Birmingham, AL) for 5 or 15 min at 37°C. Cells were harvested, washed twice with cold phosphate-buffered saline (PBS), and lysed for 30 minutes on ice with RIPA buffer (Boston Bioproducts, Boston, MA) supplemented with a protease inhibitor mix (1 tablet in 10 ml RIPA buffer, Roche, San Francisco, CA). Cell lysate was clarified by centrifugation at 10,000×g for 5 minutes, and cell extracts were fractionated by SDS-PAGE and transferred to Immun-Blot PVDF membranes (Bio-Rad laboratories, Hercules, CA). Membranes were stained with the following primary antibodies: mouse anti-IKZF3 (8B2, Ebioscience), rabbit anti-AKT antibody (40D4), anti-p-AKT (Ser473) antibody (D9E), anti-ERK1/2 antibody (137F5), anti-p-ERK1/2 antibody (Tyr202/204) (D13.14.4E), anti-p-SYK (Tyr 525/526),

anti-SYK, anti-p-NFkB P65, anti NFkB P65, anti-β-ACTIN and polyclonal anti-HSP90. Except IKZF3, all antibodies were purchased from Cell Signaling Technology (Danvers, MA). Horseradish peroxidase-coupled goat anti- rabbit or goat anti-mouse antibodies were then added (Rockland Immunochemicals Inc, Limerick, PA). The bands were visualized by using the ECL chemiluminescence Western blotting detection system (GE Healthcare, Boston, MA).

For cell fractionation experiments, nuclear and cytoplasmic extracts were obtained with the Subcellular Protein Fractionation Kit (Thermo Scientific) before western blot analysis.

Cell migration assay—For chemotaxis assays, 5×10^5 purified splenic B cells from each genotype were seeded on the upper chamber of a transwell (6.5-mm diameter, 5.0-μm pore size, Corning). 200 ng/mL CXC chemokine ligand CXCL12 (SDF-1α) (ref.250–20A, PeproTech) were next added to the lower chamber. After 3 hours of incubation at 37°C, the cells migrated to the lower part of the chamber, were flow cytometer counted for 30 seconds. The migration index was calculated as (number of cells migrated toward CXCL12 − number of cells migrated spontaneously) × 100/(total number of cells).

Intracellular calcium mobilization—Intracellular calcium flux was measured by use of the fluorogenic probe Fluo3AM (Invitrogen). 10^7 cells/mL in complete RPMI 1640 medium (Life Technologies, Woburn, MA) purified splenic B cells were incubated with 4μM Fluo3-AM and 0.02% (v/v) of Pluronic F-127 (Sigma-Aldrich) for 30 minutes at 37°C. Cells were then washed and resuspended at 5×10^6 cells/mL in complete RPMI 1640 at room temperature. Cells were kept at 37°C for 5 minutes before the acquisition of background fluorescence for 30 seconds, followed by addition of 10 μg/mL goat $F(ab')_2$ antihuman IgM (Southern Biotechnology) or 2 μM Ionomycin and data acquisition for a further 5 minutes. Calcium flux readings were analyzed using the Kinetics platform in FlowJo software (TreeStar). Fluo3AM intensity values were normalized to the average signal intensity of the 30 s baseline.

Quantitative PCR—Total RNA was extracted from mouse splenic B-cells using the Qiagen RNA purification kit (Venlo, Limburg) following manufacture's instruction. 500ng of RNA was transcribed into cDNA using the SuperscriptII reverse transcription kit (Life Technologies). The expression of mRNAs was analyzed in splenic B cells from *Ikzf3* WT, heterozygous or homozygous mutant mice using the TaqMan Gene Expression Assays probes (ThermoFischer): *Nfkbid* (Mm00549082), *Cxcr4* (Mm00516431), *Myc* (Mm00487804_m1), *Irf4* (Mm00516431_m1), *Jun* (Mm07296811_s1), *Tagap* (Mm01304651_m1). Quantitative real-time PCR was performed on a 7500 Real-time PCR system (Life Technologies). Target gene expression was normalized to the mean Ct values of the housekeeping gene *Gapdh* (Mm99999915_g1). *IKZF3* expression in human primary CLL cells was assessed by qPCR from RNA extracted from PBMC using Qiagen RNA purification kit following manufacture's instruction. 500ng of RNA was transcribed into cDNA using the SuperscriptII reverse transcription kit (Life Technologies). The expression of IKZF3 mRNAs was analyzed using the TaqMan Gene Expression Assays probes (Hs05037772_s1, ThermoFischer) and gene expression was normalized to the mean Ct

values of the housekeeping gene *Gapdh* (Hs02786624_g1). Patients were divided in high and low expressors based on median *IKZF3* expression values.

BCR sequencing—Genomic DNA was isolated using the QIAGEN DNeasy Blood & Tissue Kit (Qiagen, Valencia, CA) either from PBMC or FACS sorted CLL-like (CD5+B220+) cells from the spleen of leukemic mice and 0.5–1 μg of genomic DNA per sample was used for sequencing. Sample data was generated using the immunoSEQ Assay (Adaptive Biotechnologies, Seattle, WA). The somatically rearranged mouse *IGH* CDR3 was amplified from genomic DNA using a two-step, amplification bias-controlled multiplex PCR approach (Carlson et al., 2013; Robins et al., 2009). The first PCR consists of forward and reverse amplification primers specific for every V and J gene segment and amplifies the hypervariable complementarity-determining region 3 (CDR3) of the immune receptor locus. The second PCR adds a proprietary barcode sequence and Illumina adapter sequences. BCR repertoire analyses were performed using the immunoSEQ Analyzer 3.0 (Adaptive Biotechnologies). Sequences were subjected to analysis using IMGT/Vquest software to define all V, D and J genes as well as CDR3 sequences.

Mouse CLL transplantation—Transplantations were performed on 8–12 weeks old immunocompetent CD45.1 C57BL/6 mice (pre-conditioned with 400 rads split dose irradiation) or immunodeficient recipient NSG mice using viably cryopreserved splenocytes or peritoneal cells from donor CLL *Ikzf3* mutant heterozygous animals. Ten million total cells suspension/recipient were resuspended in 100 microliters PBS and injected intravenously into CD45.1 C57BL/6 or NSG. Disease burden in the peripheral blood, spleen and bone marrow were evaluated by flow cytometry and spleen and liver sections were examined by IHC at euthanasia.

***In vitro* drug treatments—**CLL cells from *Ikzf3*^{Het}, Eμ-TCL1 or MDR mice were resuspended in RPMI 1640 medium supplemented with 10% FBS and cultured in 96-well tissue culture plates (50,000 cells/100 μL). Cells were treated with either 5 μM Bafetinib, 5 μM Ibrutinib, 5 μM rapamycin or 5 μM gamma secretase inhibitor PF-308401. After incubation for 24 h at 37° with 5% CO2, cell viability was measured by CellTiter-Glo® Luminescent Assay and normalized by cells treated with the DMSO vehicle control.

CLL samples were resuspended in RPMI1640 medium supplemented with 10% FBS and cultured in 48-well tissue culture plates (5 ×10^6/500 μL). Cells were stimulated using soluble F(ab')2 fragment of donkey anti-human IgM antibody (10 μg/mL; Jackson ImmunoResearch, Interchim, France) with or without ibrutinib (Selleckchem, Houston, TX) at final concentration 1μM. After incubation for 24 h at 37°C with 5% CO2, cell viability was measured by Annexin V-FITC and propidium iodide (PI) staining. The percentage of response of the BCR stimulation was calculated as the difference of viable cells (Annexin V and PI negative) between the condition "anti-IgM" and the condition "anti-IgM + ibrutinib".

RNA-sequencing data generation—RNA-seq was performed on purified splenic B cells (1×10^6) from 2–3 months and 15–18 months old *Ikzf3* wild-type, heterozygous and homozygous mutant mice as well as FACS sorted B220+CD5+ CLL cells from leukemic mice or from human primary CLL samples. Cells were washed in cold PBS and total RNA

was extracted using Qiagen RNAeasy kit. For cDNA libraries construction, total RNA was quantified using the Quant-iT RiboGreen RNA Assay Kit and normalized to 5 ng/μl. Following plating, 2 μL of ERCC controls (using a 1:1000 dilution) were spiked into each sample. An aliquot of 200 ng for each sample was transferred into library preparation which uses an automated variant of the Illumina TruSeq Stranded mRNA Sample Preparation Kit. This method preserves strand orientation of the RNA transcript. It uses oligo dT beads to select mRNA from the total RNA sample, followed by heat fragmentation and cDNA synthesis from the RNA template. The resultant 400 bp cDNA then goes through dual-indexed library preparation: 'A' base addition, adapter ligation using P7 adapters, and PCR enrichment using P5 adapters. After enrichment, the libraries were quantified using Quant-iT PicoGreen (1:200 dilution). After normalizing samples to 5 ng/μL, the set was pooled and quantified using the KAPA Library Quantification Kit for Illumina Sequencing Platforms. The entire process was performed in a 96-well format and all pipetting is executed by either Agilent Bravo or Hamilton Starlet.

ChIP-sequencing data generation—Chromatin immunoprecipitation (ChIP) was performed on splenic B cells (80×10^6) from 2–3 months old *Ikzf3* wild-type and homozygous mutant mice. Cells were washed in cold PBS, fixed in 1% formaldehyde at room temperature for 10 min and the fixation reaction was quenched with 0.125M glycine for 5 min at room temperature. The cells were resuspended and lysed in 500 μl of shearing buffer containing 0.5% SDS, 10mM EDTA pH8, 50mM Tris-HCl pH8, 5mM sodium butyrate and protease inhibitor. The chromatin was sheared on the Covaris E220 sonicator, according to the following program: PIP70, 5% duty factor, 200 cycles per burst, 25 min. The sheared chromatin was diluted in 1% Triton, 2mM EDTA, 150 Mm NaCL, 20Mm Tris-HCl pH8 plus protease inhibitor. A small portion of the sheared chromatin was set aside as total input, reverse crosslinked with 1 μl of 10mg/ml RNAase for 30 min at 37°C and 5 μl of 20 mg/ml Proteinase K at 65°C overnight, purified using the Qiagen PCR purification Kit and DNA is quantify on Qubit 3.0 fluorimeter. For immunoprecipitation reaction, 25μl of Dynals magnetic beads were washed in blocking buffer (PBS plus 0.5% BSA) on a magnetic rack and incubated with 5 μg of anti-IKZF3 antibodies anti-H3K4me2, anti-H3K4me3, anti-H3K27ac, at 4°C end over end for 4 h. Conjugated beads were incubated with 25μg of diluted sheared chromatin end over end overnight at 4°C. The following day, beads were washed twice with 1ml of cold RIPA buffer, 1 ml of cold RIPA 0.3M NaCl, and with 1 ml of cold LiCl buffer. The enriched fraction of chromatin was eluted and decrosslinked from the beads by incubating with elution buffer (1% SDS, 0.1M NaHCO3), 1 μl of 10 mg/ml RNAse for 30 min at 37°C and 5 μl of 20mg/ml Proteinase K at 65°C overnight. The immunoprecipitated DNA was cleaned up using the Qiagen PCR purification Kit. Input and ChIP Libraries were prepared with the Rubicon ThruPLEX FD kit (ref. R400429, Takara Bio USA) and sequenced on Illumina NextSeq instrument to generate 75 bp single-end sequencing reads.

ATAC-seq data generation—Chromatin accessibility was assessed as previously described (Corces et al, Nat Med, 2017), without the initial DNAse digestion. Briefly, 100,000 cells were resuspended in 1 mL of cold ATAC-seq resuspension buffer (RSB; 10 mM Tris-HCl pH 7.4, 10 mM NaCl, and 3 mM MgCl2 in water). Cells were centrifuged at

maximum speed for 5 min in a pre-chilled (4°C) fixed-angle centrifuge and supernatant was carefully aspirated. Cell pellets were then resuspended in 50 μL of ATAC-seq RSB containing 0.1% NP40, 0.1% Tween-20, and 0.01% digitonin by pipetting up and down three times and incubated on ice for 3 min. After lysis, 1 mL of ATAC-seq RSB containing 0.1% Tween-20 was added, and the tubes were inverted to mix. Nuclei were then centrifuged for 5 min at maximum speed in a pre-chilled (4°C) fixed-angle centrifuge. Supernatant was removed and nuclei were resuspended in 50 μL of transposition mix (25 ul 2x TD buffer, 2.5 μL transposase (100 nM final), 16.5 μL PBS, 0.5 μL 1% digitonin, 0.5 μL 10% Tween-20, and 5 μL water) by pipetting. Samples were transposed for 30 min at 37 °C, purified with Qiagen columns, and libraries were prepared as previously described (Buenrostro et al., 2015).

Whole genome sequencing data generation—Genome sequencing was performed on flow cytometry-sorted leukemia cells from animals with CLL and matched T cells. 350 ng genomic DNA was used for library preparation. Shearing was performed acoustically using a Covaris focused-ultrasonicator, targeting 385 bp fragments. Following fragmentation, additional size selection is performed using a SPRI cleanup. DNA libraries were constructed using the KAPA Library Prep Kits (KAPA Biosystems) using palindromic forked adapters with unique 8 base index sequences embedded within the adapter (IDT). Following sample preparation, libraries were quantified using quantitative PCR (KAPA Biosystems), with probes specific to the ends of the adapters. Based on qPCR quantification, libraries were normalized to 2.2 nM and pooled into 24-plexes. Sample pools were combined with NovaSeq Cluster Amp Reagents DPX1, DPX2 and DPX3 and loaded into single lanes of a NovaSeq 6000 S4 flowcell cell using the Hamilton Starlet Liquid Handling system. Cluster amplification and sequencing were performed on NovaSeq 6000 Instruments utilizing sequencing-by-synthesis kits to produce 151 bp paired-end reads. Output from Illumina software was processed by the Picard data-processing pipeline to yield CRAM or BAM files containing demultiplexed, aggregated aligned reads.

Single Cell RNA sequencing—The sample processed for scRNA-seq was obtained from the CLL Research Consortium from a patient consented to an IRB approved research protocol. Cells were thawed and washed twice in RPMI and 10% FCS before undergoing dead cell depletion (Miltenyi Biotec; 130-090-101). CLL/B cells were purified using CD19 negative selection kit (Biolegend; 480082) and CD19 negative immune cells were purified using CD19 positive magnetic beads (Biolegend; 480106) and viable cells mixed before being washed in PBS with 0.04% BSA twice and re-suspended in PBS with 0.04% BSA (Life Technologies; AM2616) at the cell concentration of 1000 cells/μL. 17,000 cells were loaded onto a 10x Genomics Chromium instrument (10x Genomics) according to the manufacturer's instructions. The single cell RNA-seq libraries were processed using Chromium single cell 5' library & gel bead kit (10x Genomics). Quality controls for amplified cDNA libraries and final sequencing libraries were performed using Bioanalyzer High Sensitivity DNA Kit (Agilent). The libraries were normalized to 4 nM concentration and pooled in a volume ratio of 4:1. The pooled libraries were sequenced on Illumina NovaSeq S2 100 cycle platform. The sequencing parameters were: Read 1 of 28 bp, Read 2 of 91 bp and Index 1 of 8 bp.

Sequencing Data analysis—RNA-seq reads were aligned to the mouse reference genome mm10 using STAR (v2.4.0.1) (Dobin et al., 2013) and TPM (Transcripts Per Kilobase Million) value was used to measure gene expression. Differentially expressed genes were assessed using DESeq2 (Love et al., 2014) and pathway analysis is performed using Metascape (v3.0) (Zhou et al., 2019) and GSEA (v3.0) (Subramanian et al., 2005).

ChIP-seq reads were aligned to mm10 using using Bowtie2 (v2.3.4.1) (Subramanian et al., 2005) and peak detection was performed with MACS2 (v2.2.0) (Liu et al., 2008). Motif analysis was performed using RSAT motif (Nguyen et al., 2018); heatmaps and metagene plots were made using deeptools (v3.3.0) (Ramirez et al., 2016). Peak annotation was performed using GREAT (v4.0.4)(McLean et al., 2010). Integrative analysis of RNA-seq and ChIP-seq data was performed using Cistrome-GO (Li et al., 2019). Briefly, a differential expression (DE) rank RDE is derived based on the FDR representing the significance of differential expression as a result of the *Ikzf3*-L161R mutation. Secondly, a regulatory potential (RP) rank RRP is defined based on the weighted sum of mut-IKZF3 peak contributions around transcription start site (TSS). The two ranks were integrated by rank product (RDE × RRP), and the genes at the top of the list tend to have robust mut-IKZF3 binding together with significant gene expression changes, thus are more likely to be true direct targets. IGV(Robinson et al., 2011) was used to display the genomic tracks. The list of 75 BCR signaling genes was obtained from GSEA KEGG_B_CELL_RECEPTOR_SIGNALING_PATHWAY.

Whole genome sequencing raw FASTQ files were aligned to Genome Reference Consortium Mouse Build 38 (mm10) and the resulting BAM files were further processed by marking duplicated reads and recalibrating base qualities. Somatic short variant discovery of SNVs and Indels was performed using Mutect2. To perform the copy number analysis, the genomic interval list was prepared from the reference genome and read coverage counts were calculated across the intervals for all samples. A CNV panel of normal (PoN) was created using all seven of the normal samples. The tumor read coverage data was normalized using the PoN. All of the analysis was performed following the recommendation of the GATK Best Practices Workflows using GATK4 toolkit (Van der Auwera et al., 2013).

Single cell RNA sequencing data were processed using cell ranger pipeline (10x Genomics) which was analyzed using the Seurat R package (v3) (Stuart et al., 2019). Cells were filtered to have between 200 and 3000 genes/cells and less than 20,000 UMI/cell. Cells with greater than 10% mitochondrial reads were excluded. The standard processing pipeline was used including log-normalization and data-scaling. The first 30 principal components were used for downstream assays and a resolution of 0.5 for clustering. Data was visualized using UMAP. Immune cell populations were identified by cluster expression of key lineage specific markers using the FindAllMarkers function.

Luminex assay—Multiplexed measurement of individual mouse immunoglobulin isotypes (IgG1, IgG2a, IgG2b, IgG3, IgA, IgE and IgM) from sera was performed using Luminex magnetic beads technology according to the manufacturer's protocol (Antibody Isotyping 7-Plex Mouse ProcartaPlex Panel, ref. EPX070-20815-901, ThermoFisher). Cytokines and chemokines quantification from sera was performed using 26-Plex Mouse

ProcartaPlex kit (EXP260-26088-901, ThermoFisher) including: IFN-gamma; IL-12p70; IL-13; IL-1 beta; IL-2; IL-4; IL-5; IL-6; TNF-alpha; GM-CSF; IL-18; IL-10; IL-17A; IL-22; IL-23; IL-27; IL-9; GRO alpha; IP-10; MCP-1; MCP-3; MIP-1 alpha; MIP-1 beta; MIP-2; RANTES; Eotaxin.

QUANTIFICATION AND STATISTICAL ANALYSIS

Statistical analyses—Statistical analysis was performed using GraphPad Prism 6. For comparison of 3 groups, p-values were calculated with a one-way ANOVA test followed by Tukey's multiple comparison test after confirming homogeneity of standard deviation. When the standard deviations were significantly different, p-values were calculated for 2 groups at a time using a Mann-Whitney comparison test with a Bonferroni correction (nominal p-value adjusted by multiplying by the number of groups compared). Kaplan-Meier survival curves were analyzed using a log rank-test.

Supplementary Material

Refer to Web version on PubMed Central for supplementary material.

ACKNOWLEDGEMENTS

We are grateful to Drs. Paloma Cejas and Henry Long (Center for Functional Cancer Epigenetics), and Andreas Agathangelidis (Institute of Applied Biosciences, Center for Research and Technology Hellas, Thessaloniki, Greece) for constructive and valuable discussions. We acknowledge Taghi Manshouri, BS, MS (University of Texas MD Anderson Cancer Center, Houston) for expert technical support. We acknowledge Sam Pollock, Lan Nguyen, Candace Patterson, and Alicia Wong for expert project management. We thank Fara Faye Regis and the Dana-Farber Cancer Institute animal research facility technical team for excellent technical support. This study was supported by a grant from the NIH/National Cancer Institute (NIH/NCI) (P01 CA206978 and P01-CA081534). CJW acknowledges support from the NIH/NCI (R01 CA216273, U10 CA180861) and is a scholar of the Leukemia and Lymphoma Society. G.L. was a Scholar of the Fulbright and was generously supported by the Fondation de France. S.Y. is supported by a Lauri Strauss Foundation fellowship. S.H.G is a Kay Kendall Leukaemia Fund Fellow. E.T.H. is a Special Fellow of the Leukemia and Lymphoma, and a Scholar of the American Society of Hematology. S.L. is supported by the NCI Research Specialist Award (R50CA251956-01).

REFERENCES

Ahn IE, Chen Y-C, Underbayev C, Gaglione EM, Sun C, Soto S, Nierman P, Pirooznia M, and Wiestner A (2019). Diverging Clonal Evolution during Sequential Therapy with Chemoimmunotherapy Followed By BTK Inhibitors. In, (American Society of Hematology Washington, DC).

Bea S, Valdes-Mas R, Navarro A, Salaverria I, Martin-Garcia D, Jares P, Gine E, Pinyol M, Royo C, Nadeu F, et al. (2013). Landscape of somatic mutations and clonal evolution in mantle cell lymphoma. Proc Natl Acad Sci U S A 110, 18250–18255. [PubMed: 24145436]

Bichi R, Shinton SA, Martin ES, Koval A, Calin GA, Cesari R, Russo G, Hardy RR, and Croce CM (2002). Human chronic lymphocytic leukemia modeled in mouse by targeted TCL1 expression. Proc Natl Acad Sci U S A 99, 6955–6960. [PubMed: 12011454]

Billot K, Soeur J, Chereau F, Arrouss I, Merle-Beral H, Huang ME, Mazier D, Baud V, and Rebollo A (2011). Deregulation of Aiolos expression in chronic lymphocytic leukemia is associated with epigenetic modifications. Blood 117, 1917–1927. [PubMed: 21139082]

Burger JA, Burger M, and Kipps TJ (1999). Chronic lymphocytic leukemia B cells express functional CXCR4 chemokine receptors that mediate spontaneous migration beneath bone marrow stromal cells. Blood 94, 3658–3667. [PubMed: 10572077]

Burger JA, Tsukada N, Burger M, Zvaifler NJ, Dell'Aquila M, and Kipps TJ (2000). Blood-derived nurse-like cells protect chronic lymphocytic leukemia B cells from spontaneous apoptosis through stromal cell-derived factor-1. Blood 96, 2655–2663. [PubMed: 11023495]

Cancro MP, Sah AP, Levy SL, Allman DM, Schmidt MR, and Woodland RT (2001). xid mice reveal the interplay of homeostasis and Bruton's tyrosine kinase-mediated selection at multiple stages of B cell development. Int Immunol 13, 1501–1514. [PubMed: 11717191]

Cariappa A, Tang M, Parng C, Nebelitskiy E, Carroll M, Georgopoulos K, and Pillai S (2001). The follicular versus marginal zone B lymphocyte cell fate decision is regulated by Aiolos, Btk, and CD21. Immunity 14, 603–615. [PubMed: 11371362]

Carlson CS, Emerson RO, Sherwood AM, Desmarais C, Chung MW, Parsons JM, Steen MS, LaMadrid-Herrmannsfeldt MA, Williamson DW, Livingston RJ, et al. (2013). Using synthetic templates to design an unbiased multiplex PCR assay. Nat Commun 4, 2680. [PubMed: 24157944]

Chaudhuri J, and Alt FW (2004). Class-switch recombination: interplay of transcription, DNA deamination and DNA repair. Nat Rev Immunol 4, 541–552. [PubMed: 15229473]

Damle RN, Wasil T, Fais F, Ghiotto F, Valetto A, Allen SL, Buchbinder A, Budman D, Dittmar K, Kolitz J, et al. (1999). Ig V gene mutation status and CD38 expression as novel prognostic indicators in chronic lymphocytic leukemia. Blood 94, 1840–1847. [PubMed: 10477712]

Dobin A, Davis CA, Schlesinger F, Drenkow J, Zaleski C, Jha S, Batut P, Chaisson M, and Gingeras TR (2013). STAR: ultrafast universal RNA-seq aligner. Bioinformatics 29, 15–21. [PubMed: 23104886]

Dobrovolsky D, Wang ES, Morrow S, Leahy C, Faust T, Nowak RP, Donovan KA, Yang G, Li Z, Fischer ES, et al. (2019). Bruton tyrosine kinase degradation as a therapeutic strategy for cancer. Blood 133, 952–961. [PubMed: 30545835]

Duhamel M, Arrouss I, Merle-Beral H, and Rebollo A (2008). The Aiolos transcription factor is up-regulated in chronic lymphocytic leukemia. Blood 111, 3225–3228. [PubMed: 18184862]

Efanov A, Zanesi N, Nazaryan N, Santanam U, Palamarchuk A, Croce CM, and Pekarsky Y (2010). CD5+CD23+ leukemic cell populations in TCL1 transgenic mice show significantly increased proliferation and Akt phosphorylation. Leukemia 24, 970–975. [PubMed: 20357824]

Ferreira PG, Jares P, Rico D, Gomez-Lopez G, Martinez-Trillos A, Villamor N, Ecker S, Gonzalez-Perez A, Knowles DG, Monlong J, et al. (2014). Transcriptome characterization by RNA sequencing identifies a major molecular and clinical subdivision in chronic lymphocytic leukemia. Genome Res 24, 212–226. [PubMed: 24265505]

Foletta VC, Segal DH, and Cohen DR (1998). Transcriptional regulation in the immune system: all roads lead to AP-1. J Leukoc Biol 63, 139–152. [PubMed: 9468273]

Georgopoulos K, Bigby M, Wang JH, Molnar A, Wu P, Winandy S, and Sharpe A (1994). The Ikaros gene is required for the development of all lymphoid lineages. Cell 79, 143–156. [PubMed: 7923373]

Hamblin TJ, Davis Z, Gardiner A, Oscier DG, and Stevenson FK (1999). Unmutated Ig V(H) genes are associated with a more aggressive form of chronic lymphocytic leukemia. Blood 94, 1848–1854. [PubMed: 10477713]

Herold T, Jurinovic V, Metzeler KH, Boulesteix AL, Bergmann M, Seiler T, Mulaw M, Thoene S, Dufour A, Pasalic Z, et al. (2011). An eight-gene expression signature for the prediction of survival and time to treatment in chronic lymphocytic leukemia. Leukemia 25, 1639–1645. [PubMed: 21625232]

Hu Y, Zhang Z, Kashiwagi M, Yoshida T, Joshi I, Jena N, Somasundaram R, Emmanuel AO, Sigvardsson M, Fitamant J, et al. (2016). Superenhancer reprogramming drives a B-cell-epithelial transition and high-risk leukemia. Genes Dev 30, 1971–1990. [PubMed: 27664237]

Iacovelli S, Hug E, Bennardo S, Duehren-von Minden M, Gobessi S, Rinaldi A, Suljagic M, Bilbao D, Bolasco G, Eckl-Dorna J, et al. (2015). Two types of BCR interactions are positively selected during leukemia development in the Emu-TCL1 transgenic mouse model of CLL. Blood 125, 1578–1588. [PubMed: 25564405]

Klein U, Lia M, Crespo M, Siegel R, Shen Q, Mo T, Ambesi-Impiombato A, Califano A, Migliazza A, Bhagat G, and Dalla-Favera R (2010). The DLEU2/miR-15a/16–1 cluster controls B cell

proliferation and its deletion leads to chronic lymphocytic leukemia. Cancer Cell 17, 28–40. [PubMed: 20060366]

Koipally J, Renold A, Kim J, and Georgopoulos K (1999). Repression by Ikaros and Aiolos is mediated through histone deacetylase complexes. EMBO J 18, 3090–3100. [PubMed: 10357820]

Kuleshov MV, Jones MR, Rouillard AD, Fernandez NF, Duan Q, Wang Z, Koplev S, Jenkins SL, Jagodnik KM, Lachmann A, et al. (2016). Enrichr: a comprehensive gene set enrichment analysis web server 2016 update. Nucleic acids research 44, W90–97. [PubMed: 27141961]

Landau DA, Clement K, Ziller MJ, Boyle P, Fan J, Gu H, Stevenson K, Sougnez C, Wang L, Li S, et al. (2014). Locally disordered methylation forms the basis of intratumor methylome variation in chronic lymphocytic leukemia. Cancer Cell 26, 813–825. [PubMed: 25490447]

Landau DA, Tausch E, Taylor-Weiner AN, Stewart C, Reiter JG, Bahlo J, Kluth S, Bozic I, Lawrence M, Bottcher S, et al. (2015). Mutations driving CLL and their evolution in progression and relapse. Nature 526, 525–530. [PubMed: 26466571]

Lanham S, Hamblin T, Oscier D, Ibbotson R, Stevenson F, and Packham G (2003). ifferential signaling via surface IgM is associated with VH gene mutational status and CD38 expression in chronic lymphocytic leukemia. Blood 101, 1087–1093. [PubMed: 12393552]

Li S, Wan C, Zheng R, Fan J, Dong X, Meyer CA, and Liu XS (2019). Cistrome-GO: a web server for functional enrichment analysis of transcription factor ChIP-seq peaks. Nucleic Acids Res 47, W206–W211. [PubMed: 31053864]

Li X, Xu Z, Du W, Zhang Z, Wei Y, Wang H, Zhu Z, Qin L, Wang L, Niu Q, et al. (2014). Aiolos promotes anchorage independence by silencing p66Shc transcription in cancer cells. Cancer Cell 25, 575–589. [PubMed: 24823637]

Liu Q, Fu H, Sun F, Zhang H, Tie Y, Zhu J, Xing R, Sun Z, and Zheng X (2008). miR-16 family induces cell cycle arrest by regulating multiple cell cycle genes. Nucleic Acids Res 36, 5391–5404. [PubMed: 18701644]

Love MI, Huber W, and Anders S (2014). Moderated estimation of fold change and dispersion for RNA-seq data with DESeq2. Genome Biol 15, 550. [PubMed: 25516281]

Lu G, Middleton RE, Sun H, Naniong M, Ott CJ, Mitsiades CS, Wong KK, Bradner JE, and Kaelin WG Jr. (2014). The myeloma drug lenalidomide promotes the cereblon-dependent destruction of Ikaros proteins. Science 343, 305–309. [PubMed: 24292623]

McLean CY, Bristor D, Hiller M, Clarke SL, Schaar BT, Lowe CB, Wenger AM, and Bejerano G (2010). GREAT improves functional interpretation of cis-regulatory regions. Nat Biotechnol 28, 495–501. [PubMed: 20436461]

Meijers RWJ, Muggen AF, Leon LG, de Bie M, van Dongen JJM, Hendriks RW, and Langerak AW (2020). Responsiveness of chronic lymphocytic leukemia cells to B-cell receptor stimulation is associated with low expression of regulatory molecules of the nuclear factor-kappaB pathway. Haematologica 105, 182–192. [PubMed: 31097630]

Molnar A, and Georgopoulos K (1994). The Ikaros gene encodes a family of functionally diverse zinc finger DNA-binding proteins. Mol Cell Biol 14, 8292–8303. [PubMed: 7969165]

Morgan B, Sun L, Avitahl N, Andrikopoulos K, Ikeda T, Gonzales E, Wu P, Neben S, and Georgopoulos K (1997). Aiolos, a lymphoid restricted transcription factor that interacts with Ikaros to regulate lymphocyte differentiation. The EMBO journal 16, 2004–2013. [PubMed: 9155026]

Morin RD, Mendez-Lago M, Mungall AJ, Goya R, Mungall KL, Corbett RD, Johnson NA, Severson TM, Chiu R, Field M, et al. (2011). Frequent mutation of histone-modifying genes in non-Hodgkin lymphoma. Nature 476, 298–303. [PubMed: 21796119]

Muschen M (2018). Autoimmunity checkpoints as therapeutic targets in B cell malignancies. Nat Rev Cancer 18, 103–116. [PubMed: 29302068]

Nguyen NTT, Contreras-Moreira B, Castro-Mondragon JA, Santana-Garcia W, Ossio R, Robles-Espinoza CD, Bahin M, Collombet S, Vincens P, Thieffry D, et al. (2018). RSAT 2018: regulatory sequence analysis tools 20th anniversary. Nucleic acids research 46, W209–W214. [PubMed: 29722874]

Nuckel H, Frey UH, Sellmann L, Collins CH, Duhrsen U, and Siffert W (2009). The IKZF3 (Aiolos) transcription factor is highly upregulated and inversely correlated with clinical progression in chronic lymphocytic leukaemia. Br J Haematol 144, 268–270. [PubMed: 19016725]

Puente XS, Bea S, Valdes-Mas R, Villamor N, Gutierrez-Abril J, Martin-Subero JI, Munar M, Rubio-Perez C, Jares P, Aymerich M, et al. (2015). Non-coding recurrent mutations in chronic lymphocytic leukaemia. Nature 526, 519–524. [PubMed: 26200345]

Ramirez F, Ryan DP, Gruning B, Bhardwaj V, Kilpert F, Richter AS, Heyne S, Dundar F, and Manke T (2016). deepTools2: a next generation web server for deep-sequencing data analysis. Nucleic acids research 44, W160–165. [PubMed: 27079975]

Robins HS, Campregher PV, Srivastava SK, Wacher A, Turtle CJ, Kahsai O, Riddell SR, Warren EH, and Carlson CS (2009). Comprehensive assessment of T-cell receptor beta-chain diversity in alphabeta T cells. Blood 114, 4099–4107. [PubMed: 19706884]

Robinson JT, Thorvaldsdottir H, Winckler W, Guttman M, Lander ES, Getz G, and Mesirov JP (2011). Integrative genomics viewer. Nat Biotechnol 29, 24–26. [PubMed: 21221095]

Roos-Weil D, Decaudin C, Armand M, Della-Valle V, Diop MK, Ghamlouch H, Ropars V, Herate C, Lara D, Durot E, et al. (2019). A Recurrent Activating Missense Mutation in Waldenstrom Macroglobulinemia Affects the DNA Binding of the ETS Transcription Factor SPI1 and Enhances Proliferation. Cancer Discov 9, 796–811. [PubMed: 31018969]

Schoenbeck S, McKenzie DT, and Kagnoff MF (1989). Interleukin 5 is a differentiation factor for IgA B cells. Eur J Immunol 19, 965–969. [PubMed: 2787753]

Stuart T, Butler A, Hoffman P, Hafemeister C, Papalexi E, Mauck WM 3rd, Hao Y, Stoeckius M, Smibert P, and Satija R (2019). Comprehensive Integration of Single-Cell Data. Cell 177, 1888–1902 e1821. [PubMed: 31178118]

Subramanian A, Tamayo P, Mootha VK, Mukherjee S, Ebert BL, Gillette MA, Paulovich A, Pomeroy SL, Golub TR, Lander ES, and Mesirov JP (2005). Gene set enrichment analysis: a knowledge-based approach for interpreting genome-wide expression profiles. Proc Natl Acad Sci U S A 102, 15545–15550. [PubMed: 16199517]

Tamehiro N, Nishida K, Yanobu-Takanashi R, Goto M, Okamura T, and Suzuki H (2017). T-cell activation RhoGTPase-activating protein plays an important role in TH17-cell differentiation. Immunology and cell biology 95, 729–735. [PubMed: 28462950]

Taylor J, Sendino M, Gorelick AN, Pastore A, Chang MT, Penson AV, Gavrila EI, Stewart C, Melnik EM, Herrejon Chavez F, et al. (2019). Altered Nuclear Export Signal Recognition as a Driver of Oncogenesis. Cancer Discov 9, 1452–1467. [PubMed: 31285298]

Touma M, Keskin DB, Shiroki F, Saito I, Koyasu S, Reinherz EL, and Clayton LK (2011). Impaired B cell development and function in the absence of IkappaBNS. J Immunol 187, 3942–3952. [PubMed: 21900180]

Van der Auwera GA, Carneiro MO, Hartl C, Poplin R, Del Angel G, Levy-Moonshine A, Jordan T, Shakir K, Roazen D, Thibault J, et al. (2013). From FastQ data to high confidence variant calls: the Genome Analysis Toolkit best practices pipeline. Current protocols in bioinformatics 43, 11 10 11–11 10 33. [PubMed: 25431634]

Wang JH, Avitahl N, Cariappa A, Friedrich C, Ikeda T, Renold A, Andrikopoulos K, Liang L, Pillai S, Morgan BA, and Georgopoulos K (1998). Aiolos regulates B cell activation and maturation to effector state. Immunity 9, 543–553. [PubMed: 9806640]

Wang L, Brooks AN, Fan J, Wan Y, Gambe R, Li S, Hergert S, Yin S, Freeman SS, Levin JZ, et al. (2016). Transcriptomic Characterization of SF3B1 Mutation Reveals Its Pleiotropic Effects in Chronic Lymphocytic Leukemia. Cancer Cell 30, 750–763. [PubMed: 27818134]

Woroniecka R, Rymkiewicz G, Grygalewicz B, Blachnio K, Rygier J, Jarmuz-Szymczak M, Ratajczak B, and Pienkowska-Grela B (2015). Cytogenetic and flow cytometry evaluation of Richter syndrome reveals MYC, CDKN2A, IGH alterations with loss of CD52, CD62L and increase of CD71 antigen expression as the most frequent recurrent abnormalities. Am J Clin Pathol 143, 25–35. [PubMed: 25511139]

Yamanashi Y, Kakiuchi T, Mizuguchi J, Yamamoto T, and Toyoshima K (1991). Association of B cell antigen receptor with protein tyrosine kinase Lyn. Science 251, 192–194. [PubMed: 1702903]

Yan XJ, Albesiano E, Zanesi N, Yancopoulos S, Sawyer A, Romano E, Petlickovski A, Efremov DG, Croce CM, and Chiorazzi N (2006). B cell receptors in TCL1 transgenic mice resemble those of aggressive, treatment-resistant human chronic lymphocytic leukemia. Proc Natl Acad Sci U S A 103, 11713–11718. [PubMed: 16864779]

Yin S, Gambe RG, Sun J, Martinez AZ, Cartun ZJ, Regis FFD, Wan Y, Fan J, Brooks AN, Herman SEM, et al. (2019). A Murine Model of Chronic Lymphocytic Leukemia Based on B Cell-Restricted Expression of Sf3b1 Mutation and Atm Deletion. Cancer Cell 35, 283–296.e285. [PubMed: 30712845]

Yoshimi A, Lin KT, Wiseman DH, Rahman MA, Pastore A, Wang B, Lee SC, Micol JB, Zhang XJ, de Botton S, et al. (2019). Coordinated alterations in RNA splicing and epigenetic regulation drive leukaemogenesis. Nature 574, 273–277. [PubMed: 31578525]

Zanesi N, Balatti V, Riordan J, Burch A, Rizzotto L, Palamarchuk A, Cascione L, Lagana A, Dupuy AJ, Croce CM, and Pekarsky Y (2013). A Sleeping Beauty screen reveals NF-kB activation in CLL mouse model. Blood 121, 4355–4358. [PubMed: 23591791]

Zhou Y, Zhou B, Pache L, Chang M, Khodabakhshi AH, Tanaseichuk O, Benner C, and Chanda SK (2019). Metascape provides a biologist-oriented resource for the analysis of systems-level datasets. Nature communications 10, 1523.

HIGHLIGHTS

- *Ikzf3* mutation leads to CLL-like development with 40% penetrance in elderly mice
- Mutant IKZF3 acts as a transcriptional activator of BCR/NF-κB signaling genes
- Mutant IKZF3 leads to hyperactive BCR signaling and BCR inhibitor resistance
- *IKZF3* L162R phenocopies IKZF3 overexpression in primary CLL cells

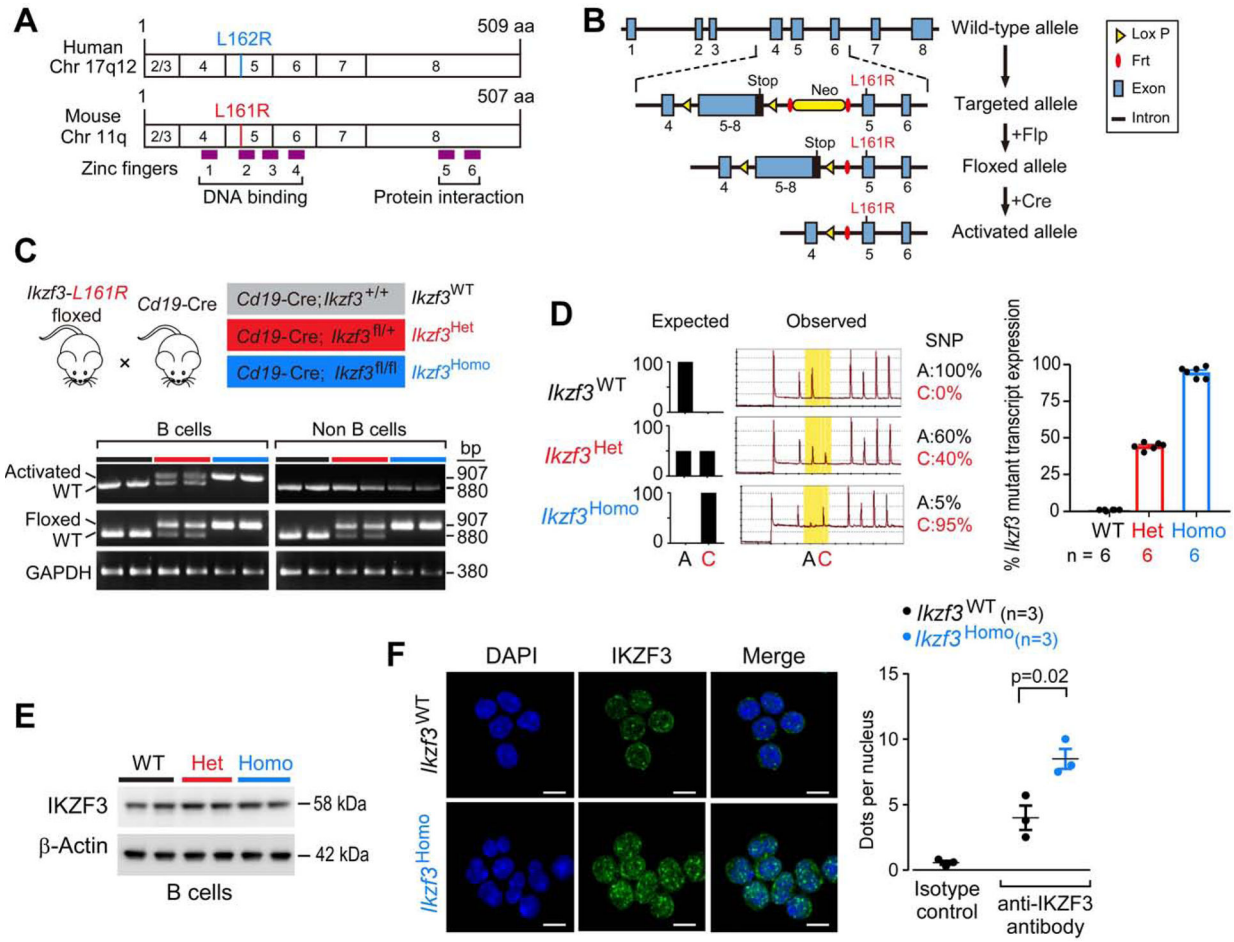

Figure 1: Conditional expression of *Ikzf3*-L161R mutation in a mouse model.

(A) Schematic representation of human and murine *IKZF3* gene with the exons, the corresponding zinc finger domains (Zf) and the position of the homologous mutation.

(B) Allele knock-in strategy.

(C) Schema of the breeding strategy. Presence of the activated *Ikzf3-L161R* allele was restricted in B-cell DNA as detected by DNA PCR.

(D) The percentage of WT and mutant Ikzf3 alleles from pyrosequencing profiles are shown.

(E) Western blot of IKZF3 protein in *Ikzf3*^{WT}, *Ikzf3*^{Het} and *Ikzf3*^{Homo} B cells.

(F) Left, immunofluorescence staining of IKZF3 WT in *Ikzf3*^{WT} B cells and of IKZF3 L161R in *Ikzf3*^{Homo} B cells. Right, nuclear dot density in *Ikzf3*^{WT} and *Ikzf3*^{Homo} B cells. The nuclear dots density was quantified using ImageJ software. Data represent the mean number of dots per nucleus counted on 100 cells in 3 *Ikzf3*^{WT} and 3 *Ikzf3*^{Homo} mice. Scale bar: 10μm.

See also Figure S1.

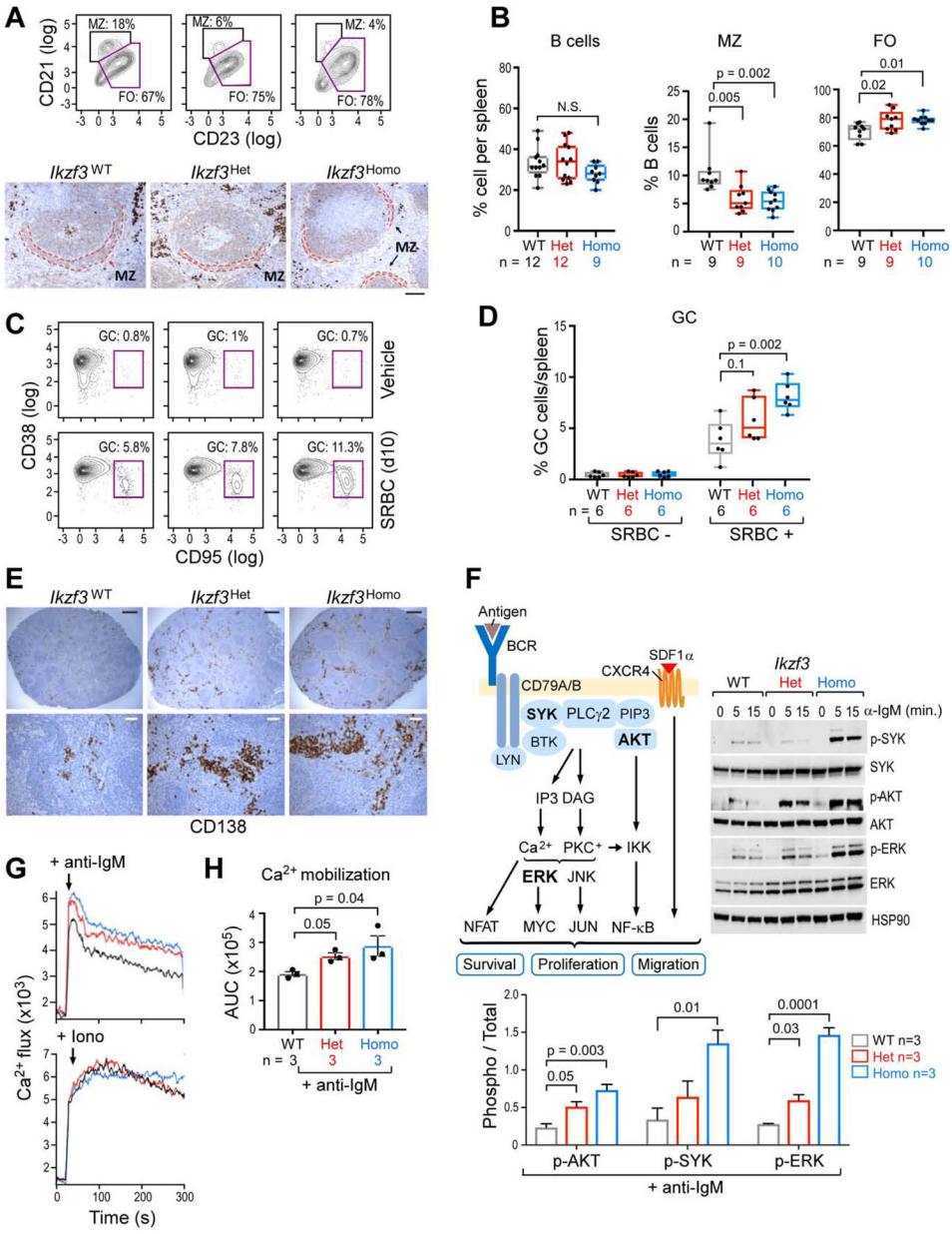

Figure 2: *Ikzf3* mutant mice have an abnormal splenic B cell development and function

(A) Top, representative FACS plot analysis of marginal zone B cells (MZ) and follicular B cells (FO) from the total splenocytes suspension. Bottom, representative immunohistochemical staining of spleen sections from *Ikzf3*^{WT}, *Ikzf3*^{Het} and *Ikzf3*^{Homo} mice (3 months of age). Red dash lines indicate marginal zone. Scale bar: 200μm.

(B) Boxplot with an inter-quartile range represent the percentages of B cells per spleens and different B-cell populations in the spleens are shown. FO: follicular B-cells, MZ: marginal zone B-cells. Median (line inside the box), 25th (bottom line) and the 75th quartile (upper line) are indicated; whiskers mark the full range of measurements. Data were compaired using one-way ANOVA followed by Tukey's multiple comparison test.

(C) Representative FACS plot analysis of germinal center B cells (GC) from the total splenocytes suspension 10 days after immunization with sheep red blood cells (SRBC) or with the vehicle.
(D) The percentage of germinal centers B cells per spleen 10 days after immunization with SRBC or with the vehicle. Data are represented and compared as per panel (B).
(E) Representative immunohistochemical staining of spleen sections from immunized mice (3 months of age). Scale bars, black: 500 μm, white: 50 μm.
(F) top left, BCR signaling pathway schema. Right, Representative Western Blot of BCR signaling components in splenic B cells 5 min following BCR stimulation with anti-IgM. Data represent Mean±SEM and were compaired using one-way ANOVA followed by Tukey's multiple comparison test.
(G) Calcium flux measurements following anti-IgM stimulation (top) and with ionomycin (bottom) of splenic B cells.
(H) Area under the curve (AUC) of the calcium flux in B cells stimulated with anti-IgM. Data represent Mean±SEM and were compaired using one-way ANOVA followed by Tukey's multiple comparison test.
See also Figure S1 and S2.

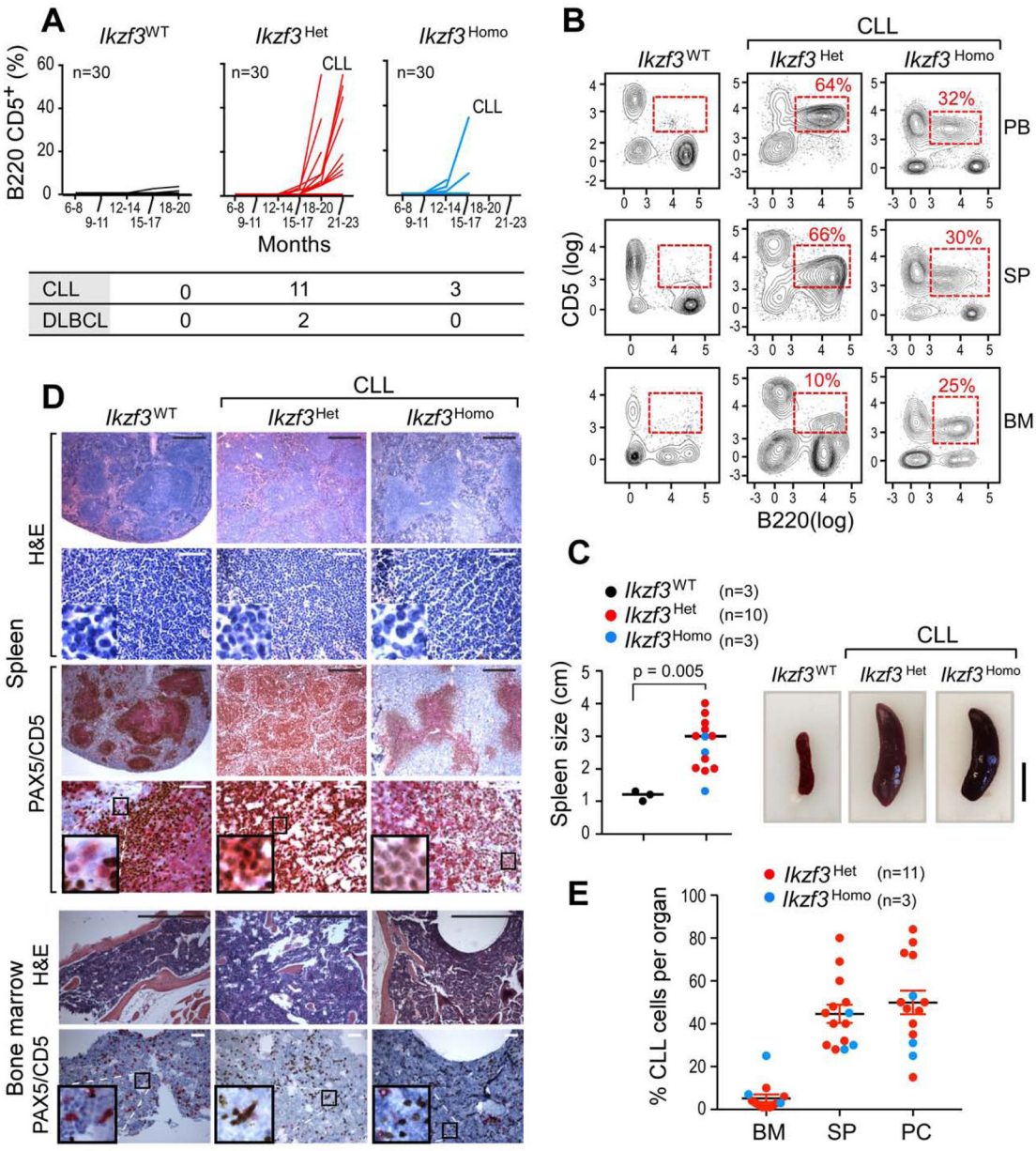

Figure 3: Conditional expression of *Ikzf3*-L161R mutation is sufficient to generate murine CLL-like disease.

(A) Top, Detection of B220+CD5+ cells in peripheral blood. Bottom, number of cases of CLL and diffuse large B cell lymphoma (DLBCL) in each group.

(B) Flow cytometry analysis of B220+ CD5+ cells within peripheral blood (PB), spleen (SP) and bone marrow (BM) of *Ikzf3*^{WT}, *Ikzf3*^{Het}-CLL and *Ikzf3*^{Homo}-CLL mice.

(C) Left, size of the spleens of leukemic and non-leukemic mice. Right, representative pictures of spleens of the indicated genotypes. Median values are indicated by horizontal lines; p value, unpaired t test.

(D) HE staining and immunohistochemical staining of CD5^{+}PAX5^{+} cells in the spleen and the bone marrow tissues. Representative spleens are shown for each group of mice. Scale bars, black: 500 μm, white: 50μm.

(E) Percentage (Mean ± SEM) of CLL cells in bone marrow (BM), spleen (SP) and peritoneum cavity (PC) of CLL mice.
See also Figure S3 and Table S1.

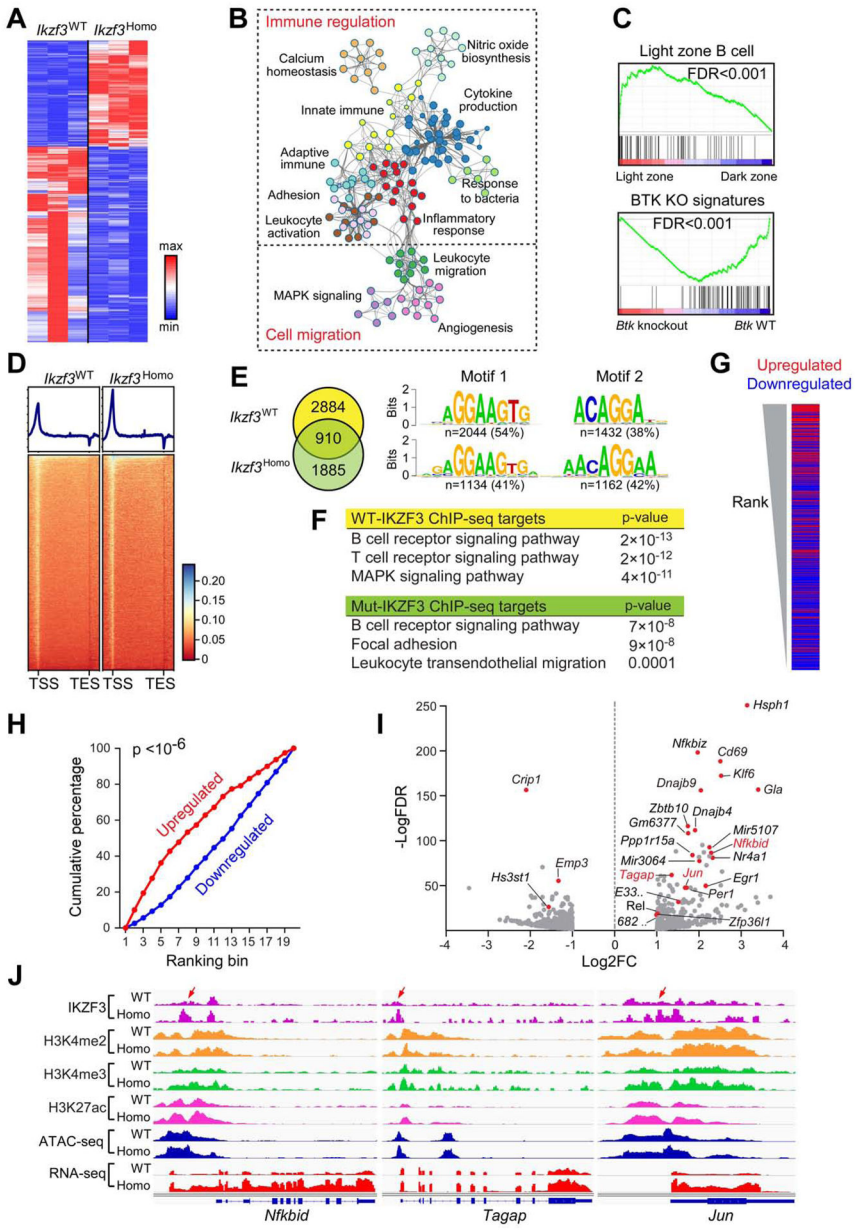

Figure 4 : *Ikzf3* mutation alters DNA binding and target selection.

(A) Heatmap shows normalized expression of significantly deregulated genes between *Ikzf3*^{Homo} and *Ikzf3*^{WT} B cells (n = 3 per group).

(B) Network enrichment analysis of the differentially expressed genes using Metascape. Functional categories are represented by different colors, and each circle denotes an enriched term (see Table S3).

(C) GSEA for enrichment of light zone B cell genes and *Btk* pathway targets in *Ikzf3*^{Homo} versus *Ikzf3*^{WT} B cells.

(D) Heatmap of IKZF3 ChIP-seq signals around all genes in the genome. TSS: transcription start site; TES: transcription end site.

(E) Venn diagram of the overlap of IKZF3 peaks between *Ikzf3*^{Homo} and *Ikzf3*^{WT} B cells. The DNA sequence motifs of the peaks, and the number of peaks containing the motif are shown.

(F) Top KEGG pathways significantly enriched for genes with WT- or mut-IKZF3 peaks.

(G) Significantly changed genes, ranked by Cistrome-GO ranks (red - upregulated genes, blue-downregulated genes).

(H) Cumulative distribution of up- or down-regulated genes based on Cistrome-GO ranks. Genes were equally divided into 19 bins, with the top most-ranked genes in Bin 1.

(I) Log_2 fold change versus logFDR of all differentially expressed genes. Red dots - topmost ranked genes per Cistrome-GO.

(J) IGV tracks of ChIP-seq, ATAC-seq and RNA-seq coverage of the top three target genes in *Ikzf3*^{WT} and *Ikzf3*^{Homo} B cells. Red arrows - the novel/enhanced binding sites of mut-IKZF3.

See also Figure S4 and Table S2–S3.

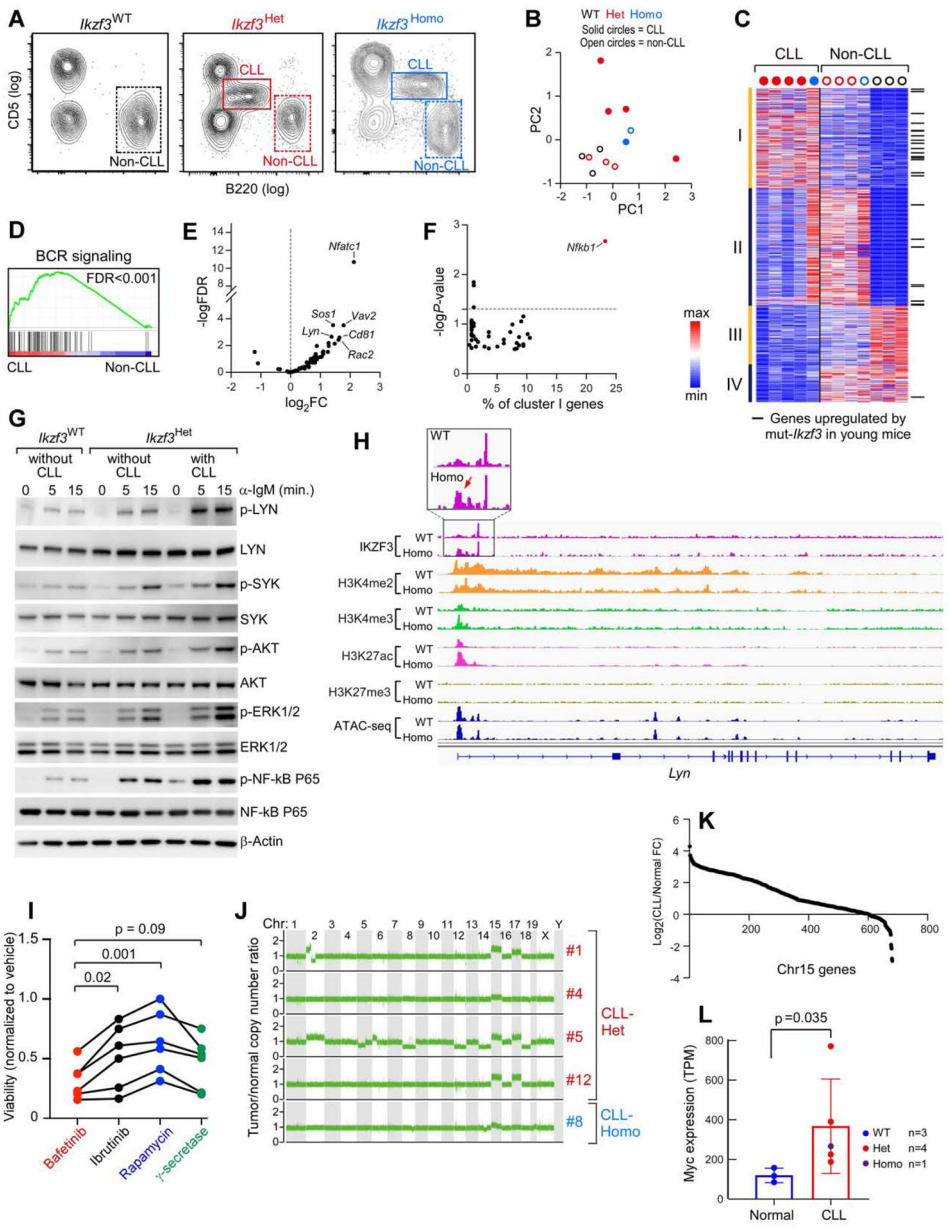

Figure 5 : *Ikzf3* mutation activates BCR signaling in CLL-like cells.

(A) Representative gating strategies for flow cytometric sorting of non-CLL B cells ($B220^+$ $CD5^-$) and CLL-like cells ($B220^+$ $CD5^+$) from splenocytes, used for RNA-seq analysis.

(B) PCA analysis of gene expression profiles from the collected cells.

(C) Normalized expression of significantly deregulated genes between CLL-like cells and $Ikzf3^{WT}$ B cells (n=3–5 per group). Genes were divided into four groups based on K-means cluster. Black lines-significantly upregulated genes in $Ikzf3^{Homo}$ versus $Ikzf3^{WT}$ B cells from 3 months old mice.

(D) GSEA analysis for enrichment of BCR signaling genes in CLL-like cells versus non-CLL cells from the same mice.

(E) Log_2FC change versus logFDR of all BCR signaling genes. FC, fold change.

(F) Scatterplot of transcription factors predicted to regulate cluster I genes (% of cluster I genes regulated by certain transcription factor and the logP-value of enrichment). Line indicates p-value of 0.05.

(G) Western Blot analysis of BCR signaling activity B cells from *Ikzf3*^{WT}, *Ikzf3*^{Het} mice (without CLL) or from *Ikzf3*^{Het} CLL cells, 5 min following BCR stimulation with anti-IgM. β-ACTIN was probed as a loading control.

(H) IGV tracks of ChIP-seq and ATAC-seq coverage of the *Lyn* gene in *Ikzf3*^{WT} and *Ikzf3*^{Homo} B cells.

(I) Viability of cells treated for 24 h with bafetinib (5 μM), ibrutinib (5 μM), rapamycin (5 μM) or γ-secretase inhibitor (5 μM). Data were compared using a one-sided paired t test followed by Bonferroni correction.

(J) Chromosomal copy-number variants in mut-*Ikzf3* CLL cells detected using whole-genome sequencing. The copy-number ratios to normal tissue are shown.

(K) Changes in gene expression of Chr15 genes between CLL and normal B cells. Genes were sorted by CLL/normal expression fold change (FC).

(L) Expression of *Myc* in normal B cells and CLL cells by RNA-seq.

See also Figure S5 and Table S4–S5.

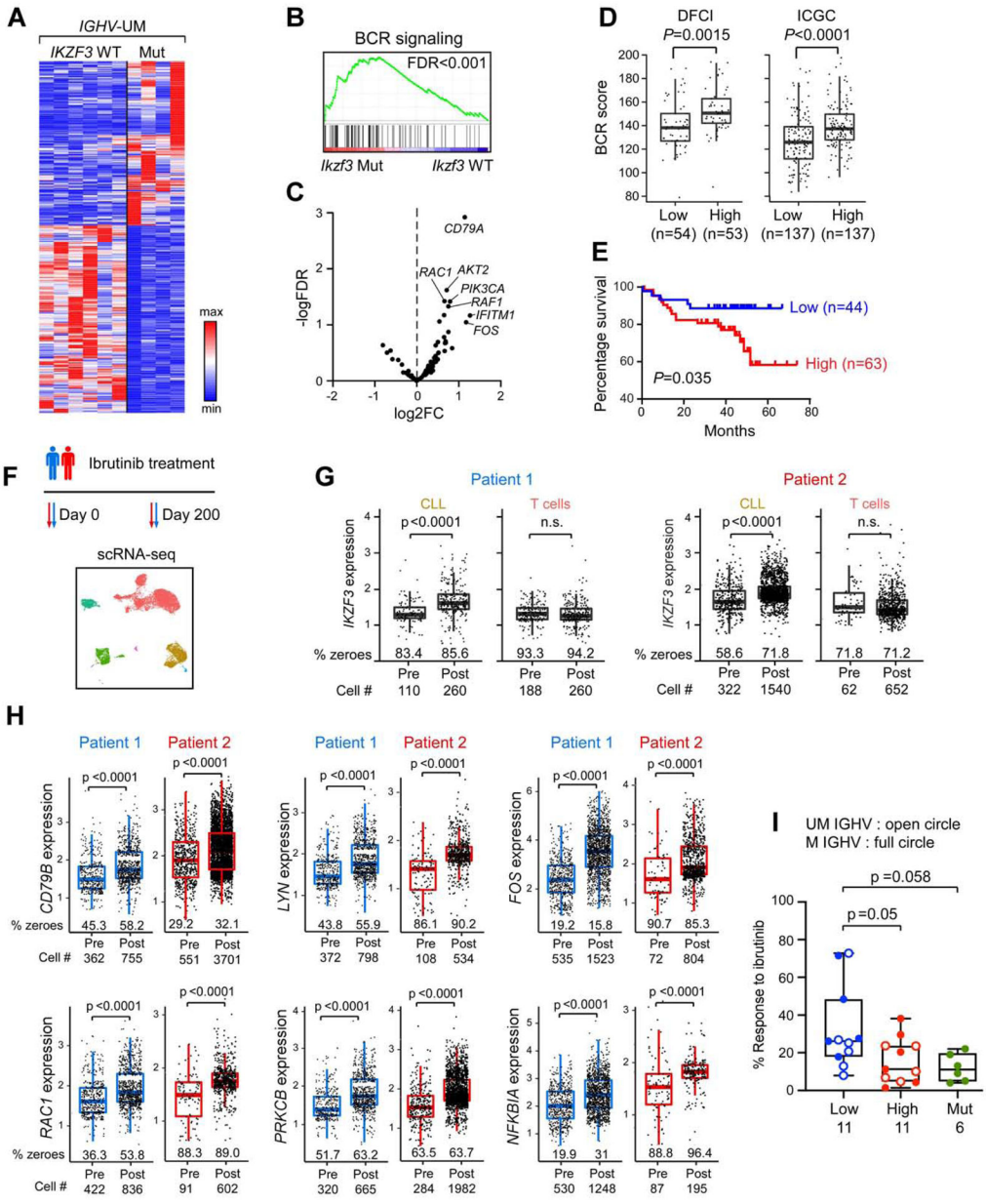

Figure 6: *IKZF3* as a key regulator of BCR signaling and drug response in human CLLs

(A) Heatmap shows normalized expression of significantly changed genes between *IKZF3* WT (n=6) and mut (n=4) CLLs.

(B) GSEA analysis for enrichment of BCR signaling genes in *IKZF3* WT versus *IKZF3* mutant human primary CLL cells.

(C) Log_2 fold change versus logFDR of differential gene expression between WT and mut CLLs; BCR signaling genes are labelled.

(D) Boxplot with an inter-quartile range (IQR) indicate BCR scores (defined by mean expression (TPM) of 75 BCR signaling genes) in CLL patients with high or low *IKZF3* expression (defined by median) in two independent cohorts are shown. Median is

represented as a line inside the box, and the 25th and the 75th quartiles are indicated by lines at the bottom and top of the box; and whiskers indicate the range of 1.5*IQR.

(E) Kaplan-Meier survival curve of CLL patients with high or low *IKZF3* expression. Data were obtained from GSE22762.

(F) Schematic of scRNA-seq experiment of patients undergoing ibrutinib treatment.

(G) *IKZF3* expression in different cell types pre- and post-treatment are shown. “%zeroes” represents the percent of total cells samples with zero expression within the population. Cell # indicates the number of cells with signals of the particular gene and are included in the box plot.

(H) Expression of different BCR signaling genes in CLL cells pre- and post-treatment are shown.

(I) Boxplot with an interquartile range (IQR) indicate response of primary CLL cells with either low, high or mutant *IKZF3* expression to ibrutinib *in vitro* following BCR stimulation with anti-IgM for 24h. Median is represented as a line inside the box, and the 25th and the 75th quartile are indicated by lines at the bottom and top of the box; whiskers indicate the full range of measurements. Data were compaired using one-way ANOVA followed by Tukey’s multiple comparison test.

See also Figure S6 and Table S6.

REAGENT or RESOURCE	SOURCE	IDENTIFIER
Antibodies		
anti-CD5 (FITC) - Flow cytometry	Biolegend	Cat# 100606; RRID: AB_312734
anti-CD11b (APC-Cy7) - Flow cytometry	Biolegend	Cat# 101212; RRID: AB_312794
anti-B220 (Pacific Blue) - Flow cytometry	Biolegend	Cat# 103227; RRID: AB_492876
anti-CD3 (APC) - Flow cytometry	Biolegend	Cat# 100236; RRID: AB_2561456
anti-Igκ (PE) - Flow cytometry	Biolegend	Cat# 409506; RRID: AB_2563581
anti-CD43 (PE) - Flow cytometry	BD Pharmingen	Cat# 560663; RRID: AB_1727479
anti-IL-7R (BV711) - Flow cytometry	Biolegend	Cat# 135035; RRID: AB_2564577
anti-CD93 (BV650) - Flow cytometry	Biolegend	Cat# 136509; RRID: AB_2275879
anti-IgM (PeCy7) - Flow cytometry	Biolegend	Cat# 408610; RRID: AB_2728434
anti-IgD (APC-C7) - Flow cytometry	Biolegend	Cat# 405716; RRID: AB_10662544
anti-B220 (BV421) - Flow cytometry	Biolegend	Cat# 103239; RRID: AB_10933424
anti-CD21 (BV510) - Flow cytometry	BD Biosciences	Cat# 747764
anti-CD23 (BV786) - Flow cytometry	BD Biosciences	Cat# 563988; RRID:AB_2738526
anti-CD11b (PerCP-Cy5.5) - Flow cytometry	BioLegend	Cat# 101227; RRID: AB_893233
anti-CD95 (PE) - Flow cytometry	BioLegend	Cat# 152607; RRID: AB_2632903
anti-CD38 (APC) - Flow cytometry	BioLegend	Cat# 102711; RRID: AB_312932
anti-CD138 (BV421) - Flow cytometry	BioLegend	Cat# 142507; RRID: AB_11204257
anti-TACI (PE) - Flow cytometry	ebioscience	Cat# 12-5942-81; RRID: AB_837121
anti-B220 (PerCP-Cy5.5) - Flow cytometry	ebioscience	Cat# 45-0452-82; RRID: AB_1107006
anti-CD19 (APC-Cy) - Flow cytometry	BD Pharmingen	Cat# 553783; RRID:AB_395047
anti-Annexin V (FITC) - Flow cytometry	BD Biosciences	Cat# 556420
anti-IKZF3 (9D10) - ChIP seq	Milipore	Cat# MABE911
anti-H3K4me2 - ChIP seq	Milipore	Cat# 07–030; RRID:AB_310342
anti-H3K4me3 - ChIP seq	Abcam	Cat# 8580
anti-H3K27me3 - ChIP seq	Cell signaling technologies	Cat# 9733S; RRID:AB_2616029
anti-H3K27ac - ChIP seq	Diagenode	Cat# C15410196; RRID:AB_2637079
anti-IKZF3 (8B2) - Western Blot, Immunofluorescence	Ebioscience	Cat# 14-5789-82; RRID: AB_10734227
anti-AKT (40D4) - Western Blot	Cell Signaling Technology	Cat# 2920; RRID: AB_1147620
anti-p-AKT S473 (D9E) - Western Blot	Cell Signaling Technology	Cat# 4060; RRID: AB_2315049
anti-ERK1/2 (137F5) - Western Blot	Cell Signaling Technology	Cat# 4695; RRID: AB_390779
anti-p-ERK1/2 (D13.14.4E) - Western Blot	Cell Signaling Technology	Cat# 4094S; RRID: AB_10694057
anti-p-SYK (Tyr 525/526) - Western Blot	Cell Signaling Technology	Cat# 2711; RRID:AB_2197215
anti-SYK - Western Blot	Cell Signaling Technology	Cat# 2712; RRID:AB_2197223
anti NFkB P65 - Western Blot	Cell Signaling Technology	Cat# 8242; RRID:AB_10859369
anti-β-ACTIN - Western Blot	Cell Signaling Technology	Cat# 4967; RRID:AB_330288

REAGENT or RESOURCE	SOURCE	IDENTIFIER
anti-HSP90 - Western Blot	Cell Signaling Technology	Cat# 4874; RRID:AB_2121214
anti-p- NFkB P65 - Western Blot	Cell Signaling Technology	Cat# 3033; RRID:AB_331284
anti-LYN - Western Blot	Cell Signaling Technology	Cat# 2796S; RRID:AB_2138391
anti-p-LYN - Western Blot	Abcam	Cat# ab226778
anti-BCL6 - Immunohistochemistry	Santa Cruz	Cat# sc-858; RRID:AB_2063450
anti-BCL2 - Immunohistochemistry	Abcam	Cat# ab182858; RRID:AB_2715467
anti-Ki-67 - Immunohistochemistry	Vector Lab	Cat# VP-K451; RRID:AB_2314701
anti-CD19 - Immunohistochemistry	Cell Signaling Technology	Cat# 90176; RRID:AB_2800152
anti-CD5 - Immunohistochemistry	Sino Biological	Cat# 50403-RP02
anti-PAX5 - Immunohistochemistry	Cell Signaling Technology	Cat# 12709; RRID:AB_2798001
anti-HnRNAP1 (8B2) - Western Blot	ebioscience	Cat# 14-5789-82
Biological Samples		
Human CLL Primary Peripheral Blood	Avicenne Hospital, DFCI, MDACC	N/A
Chemicals, Peptides, and Recombinant Proteins		
ACK buffer	Life Technologie	Cat# A10492–01
recombinant murine CXCL12(SDF1α)	PeproTech	Cat# 250–20A
Fluoro3AM probe	Invitrogen	Cat# F1241
Pluronic F-127	Sigma Aldrich	Cat# P2443
Fresh sheep red blood cells	Innovative Research	Cat# IC100–0210
goat F(ab')2 anti-mouse IgM	Southern biotech	Cat# 1023–01
donkey F(ab')2 anti-Human IgM	Jackson Immunoresearch	Cat# 709-006-073
Ibrutinib	Selleckchem	Cat# S2680
Bafetinib	Selleckchem	Cat# S1369
Rapamycin	MedChem express	Cat# AY-22989
PF-3084014	MedChem express	Cat# HY-15185
Annexin V 10X Binding Buffer	BD Biosciences	Cat# 556454
Propidium iodide	BD Biosciences	Cat # 556463
Critical Commercial Assays		
RNAeasy Kit	Qiagen	Cat# 74104
DNeasy Blood & Tissue Kit	Qiagen	Cat# 69504
PyroMark Gold Q96	Qiagen	Cat# 972804
MACS mouse B cell Isolation Kit	Miltenyi Biotec	Cat# 130-090-862
ThruPLEX FD kit	Takara Bio	Cat# R400429
Antibody Isotyping 7-Plex Mouse ProcartaPlex panel	ThermoFisher	Cat# EXP070-20815-901
26-Plex Mouse ProcartaPlex Kit	ThermoFisher	Cat# EXP26088–901
Dead cell removal kit	Miltenyi Biotec	Cat# 130-090-101
MojoSort™ Human Pan B Cell Isolation Kit	Biolegend	Cat# 480082
Chromium single cell 5' library and gel bead kit	10X genomics	Cat# NC1738507
Bioanalyzer High Sensitivity DNA kit	Aligent	Cat# 5067–4627

REAGENT or RESOURCE	SOURCE	IDENTIFIER
Cell titer Glo	Promega	Cat# G7571
KAPA Hyper Prep Kit	Roche	Cat# KK8505
NovaSeq 6000 SP Reagent Kit	Illumina	Cat# 20027464
TDE1 tagmentation enzyme	Illumina	Cat# FC-121–1030
Deposited Data		
Murine RNA-seq, ChIP-seq and ATAC-seq data	This paper	GEO: GSE143711
Human RNA-seq data	This paper	dbGAP : phs2335.v1
Experimental Models: Organisms/Strains		
Mouse: Cd19cre (B6.129P2(C)- *Cd19*$^{tm1(cre)Cgn}$)	The Jackson Laboratory	Ref 6785
Mouse: CD45.1 (B6.SJL-*Ptprc* ^{a} *Pepc*^{b}/BoyJ)	The Jackson Laboratory	Ref 2014
Mouse: NSG (NOD.Cg-*Prkdc*^{scid} *Il2rg*^{tm1Wjl}/SzJ)	The Jackson Laboratory	Ref 5557
Mouse: *Ikzf3* $^{fl/+}$ (C57BL/6 background)	The Jackson Laboratory	Ref 35514
Oligonucleotides		
Nfkbid (murine) (commercial Taqman probes)	Thermo Fisher	Mm00549082_m1
Cxcr4 (murine) (commercial Taqman probes)	Thermo Fisher	Mm00516431_m1
Myc (murine) (commercial Taqman probes)	Thermo Fisher	Mm00487804_m1
Irf4 (murine) (commercial Taqman probes)	Thermo Fisher	Mm00516431_m1
Jun (murine) (commercial Taqman probes)	Thermo Fisher	Mm07296811_s1
Tagap (murine) (commercial Taqman probes)	Thermo Fisher	Mm01304651_m1
Ikzf3 (murine) (commercial Taqman probes)	Thermo Fisher	Mm01306721_m1
Gapdh (murine) (commercial Taqman probes)	Thermo Fisher	Mm99999915_g1
Gapdh (human) (commercial Taqman probes)	Thermo Fisher	Hs02786624_g1
Ikzf3 (human) (commercial Taqman probes)	Thermo Fisher	Hs05037772_s1
Genotyping primer for floxed allele in *Ikzf3* mutant mice : Forward 5'-CTTGACTCTGTGAGTCCGTTTTGC	This paper	N/A
Genotyping primer for floxed allele in *Ikzf3* mutant mice: Forward 5'-CAGTGACACAGATCGCTTGGGAAC	This paper	N/A
Genotyping primer for activated allele in Ikzf3 mutant mice : Reverse 5'TGCTGCTCTCCAGACACAAGGC	This paper	N/A
Genotyping primer for activated allele in Ikzf3 mutant mice : Reverse 5'TCATGATGAGTCCCATGCCACGC	This paper	N/A
Pyrosequencing primer for murine *Ikzf3* : Forward 5'ATCAGTGTGGGGCATCTTT	This paper	N/A
Pyrosequencing primer for murine *Ikzf3* : Reverse 5'Bio-TTTTCCCCTGTGTGCAGTTTAA	This paper	N/A
Pyrosequencing probe for murine Ikzf3: 5'TACTCAGAAAGGTAACCTC.	This paper	N/A
Software and Algorithms		
FlowJo	TreeStar	N/A
GraphPad Prism version 7	GraphPad	https://www.graphpad.com/scientific-software/prism/
DESeq2	Love et al., 2014	https://bioconductor.org/packages/release/bioc/html/DESeq2.html

REAGENT or RESOURCE	SOURCE	IDENTIFIER
GSEA (v3.0)	Subramanian et al., 2005	http://software.broadinstitute.org/gsea/index.jsp
Metascape (v3.0)	Zhou et al.,2019	https://metascape.org/gp/index.html#/main/step1
Bowtie2 (v2.3.4.1)	Langmead and Salzberg, 2012	http://bowtie-bio.sourceforge.net/bowtie2/index.shtml
deepTools (v3.3.0)	Ramírez et al., 2016	https://deeptools.readthedocs.io/en/develop/
RSAT motif	Van Helden et al., 2003	http://rsat.sb-roscoff.fr
GREAT (v4.0.4)	McLean et al., 2010	http://great.stanford.edu/public/html/
Cistrome-GO	Li et al., 2019	http://go.cistrome.org
IGV	Robinson et al., 2011	http://software.broadinstitute.org/software/igv/
GATK4	Poplin et al. 2017	https://gatk.broadinstitute.org/hc/en-us